A Testbed for Design and Performance Evaluation of the Visual Localization Technique inside the Small Intestine

by

Liang Mi

A Thesis

Submitted to the Faculty

of the

WORCESTER POLYTECHNIC INSTITUTE

In partial fulfillment of the requirements for the

Degree of Master of Science

in

Electrical and Computer Engineering

by

_____

May 2014

APPROVED:

_____   _____
Prof. Kaveh Pahlavan, Dept. of ECE   Prof. Yehia Massoud, Head of Dept.
Major Thesis Advisor

_____   _____
Prof. Emmanuel Agu, Dept. of CS   Dr. Allen Levesque, Dept. of ECE

"To my family"

Liang Mi

Abstract

Wireless video capsule endoscopy (VCE) plays an increasingly important role in assisting clinical diagnoses of gastrointestinal (GI) diseases. It provides a non-invasive way to examine the entire small intestine, where other conventional endoscopic instruments can barely reach. Existing examination systems for the VCE cannot track the location of a endoscopic capsule, which prevents the physician from identifying the exact location of the abnormalities. During the eight hour examination time, the video capsule continuously keeps taking images at a frame rate up to six frame per sec, so it is possible to extract the motion information from the content of the image sequence. Several attempts have been made to develop computer vision algorithms to detect the motion of the capsule based on the small changes in the consecutive video frames and then trace the location of the capsule. However, validation of those algorithms has become a challenging topic because conducting experiments inside the human body is extremely difficult due to individual differences and legal issues. In this thesis, two validation approaches for motion tracking of the VCE are presented in detail respectively. One approach builds a physical testbed with a plastic pipe and an endoscopy camera; the other builds a virtual testbed by creating a three-dimensional virtual small intestine model to simulate the motions of the capsule. Based on the virtual testbed, a physiological factor, intestinal contraction, has been studied in terms of its influence on visual based localization algorithms and a geometric model for measuring the amount of contraction is proposed and validated. The emulated endoscopic images from the testbed have been used in support of the performance evaluation of a visual based localization algorithm for the VCE.

Acknowledgments

I would like to express my gratitude to my advisor professor Kaveh Pahlavan who has been supervising me on my research over one and a half years. During this period of time, I have grown from a fresh college student to a Master student who can work independently and with other colleagues on challenging research topics. His generous advices have been guided me toward the under beauty of the fundamental research. He considers things in a high-level perspective and he can always provide interesting ideas. He encourages people to do the things in such a way that they are interested in, they care about, because that will make everyone happy and productive at the same time.

My gratitude also goes to my parents Wei Mi and Rong Sun who have been supporting me in any sense. They regard me as their first priority forever. They always make themselves available to help me and provide a suitable environment for my growth, no matter how busy and how tired they have been during these years. Looking back to every achievement I have gained so far, none of them can be accomplished without them, including my Master degree. I would like to take this chance to convey my biggest thanks to them.

Also, I would like thank Doctor Guanqun Bao for his generous help on instructing me throughout this research, including programming in Matlab and OpenGL, writing papers, designing and implementing algorithms as well as tremendous general suggestions; professor Emmanuel Agu for his help on building my knowledge of computer graphics; professor Allen Levesque for his precious advice in editing of this thesis; and all other former and current members in the CWINS lab: Yunxing Ye, Yishuang Geng, Bader Alkandari, Jin Chen, Zhuoran Liu, Fardad Askarzadeh, Nader Bargshady for their direct and indirect help on my research work.

Thank those new members of the CWINS lab: Mingda Zhou, Guanxiong Liu,

Contents

5

List of Figures

6

7

9

List of Tables

Abbreviation

ASIFT   Affine Scale Invariant Feature Transform

BAN   Body Area Network

CT   Computer Tomography

CTC   Computer Tomography Colonography

EM   EelectroMagnetism

FDA   Food and Drug and Administration

FP   Feature Points

GF   Gastric Fiberscopy

GI   Gastro Intestinal

GPS   Global Positioning System

MRI   Magnetic Resonance and Imaging

MT   Magnetic Tracing

RF   Radio Frequency

RSS   Received Signal Strength

SIFT   Scale Invariant Feature Transform

SPECT   Single-Photon Emission Computerized Tomography

ToA   Time of Arrival

WCE   Wireless Capsule Endoscopy

VCE   Video Capsule Endoscope

VCE   Video Capsule Endoscopy

VE   Virtual Endoscopy

Chapter 1

Introduction

In this chapter, a general introduction of the video capsule endoscopy and its localization techniques are given. Section 1.1 gives a brief introduction of the evolution of video capsule endoscopy (VCE). In section 1.2, the problem of localization of video capsule endoscope (VCE) is addressed and an visual based technique - motion tracking - is introduced. The motivation and contribution of this thesis are described in section 1.3 and 1.4. The outline of this thesis is presented in section 1.5.

1.1   Introduction to Video Capsule Endoscopy

In recent years, there has been an increasingly larger trend in exploring the inside of human's digesting systems for a variety of health care applications [1]. In late 1990s, due to miniaturization, cost reduction and power dissipation deduction of semiconductor devices, it became possible to design a small, ingestible, low cost, energy efficient and harmless device that could take pictures of inside the gastrointestinal (GI) tract of the human body [2].

Traditional means of examining the GI tract involve either electromagnetic radiation (EMR) or electromagnetic field (EF or EMF) that can penetrate the human body, or a wired endoscope (push enteroscopy) inserted from the upper or lower end of GI tract. Using EMR, such as computed tomography (CT) [3] using X-ray

and single-photon emission computerized tomography (SPECT) [4] using Gamma-ray, has dramatic health hazards on human body by increasing the possibility of cells' cancerization. Using EF, such as magnetic resonance imaging (MRI) [5], is extremely expensive and not applicable for those patients who have implanted metal in their body. Traditional push endoscopy, which uses a wired camera, usually cannot examine the entire small intestine and it makes patients more or less uncomfortable during the procedure.

First introduced by Given Imaging, Yokneam, Israel in 2000, video capsule endoscopy (also called wireless video capsule endoscopy and sometimes wireless capsule endoscopy) is a noninvasive way to examine the GI tract of the human body [6]. The capsule is the size and shape of a pill and it contains a tiny camera in the front as shown in Figure 1.1a. After the capsule is swallowed by a patient, it continuously takes pictures and immediately sends them to a receiver outside the human body (as shown in Figure 1.1b). Based on the pictures, doctors can gain a better understanding of the inside environment of the GI tract [7], as shown in Figure 1.1c.

(a) Video capsule	(b) Data recording	(c) Video review
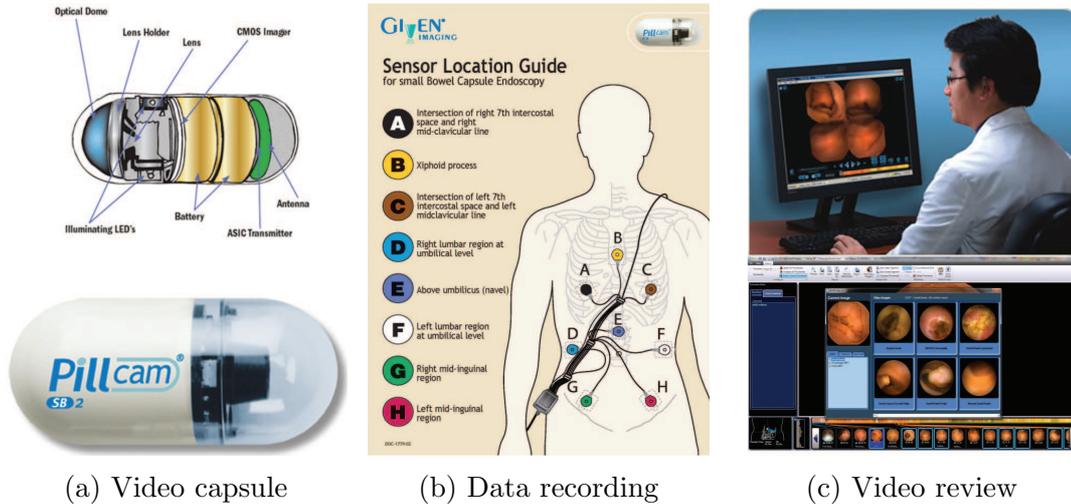
Figure 1.1: Complete procedure of VCE. Video capsule is a pill-shaped capsule with built-in camera, light-emitting diodes, video signal transmitter and battery as shown in (a); After a patient swallows the capsule, it records video and sends the data to the data recorder as shown in (b); Using a professional software, a trained physician reviews the video and considers it as reference of diagnoses (c)

The biggest contribution of the VCE is that it helps close a gap in the evaluation of the small bowel, which had been regarded as the "black box" of endoscopy for many years because wired endoscopy either gastroscopy or colonoscopy cannot reach that part of the GI tract [8] [9]. The invention of the PillCam video capsule endoscope (VCE), a small, ingestible camera, opened up a new world of explorations and diagnoses of the GI tract.

Human trials of VCE for examining the small intestine was first introduced in 2000 [10]. Since then,VCE has been playing an increasingly important role in assisting clinic diagnoses of diseases and abnormalities inside the small intestine [11]. Many research articles and clinical reports have demonstrated the usefulness of VCE in finding and diagonalizing bleeding [12] [13], ulceration [14] [15] and Crohn's disease [16] [17] and many techniques involving radio frequency (RF) [18], electromagnetism (EM) [19] and video tracking [20] [21] have been invented for automatic localization of those diseases and abnormalities [22] [4].

1.2 Localization of Video Capsule Endoscope and Motion Tracking

One of the biggest drawbacks of the VCE is its inability to locate itself. Once the patient has swallowed the video capsule, there is no way to control the motion of it without attaching other devices. The capsule is completely passively pushed by intestinal peristalsis. Most of the time the capsule moves forward; sometimes it moves backward; sometimes the capsule even flips because of the intestinal motility [23]. Thus even the VCE finds an abnormality during its transition inside the GI tract, the location of the abnormality is still absent, which to a large extent prevents the physician from administrating immediate therapeutic treatments [24].

During the past decade, researchers have made many attempts to locate the VCE with several approaches. The two most widely used approaches so far are radio

(a) RF localization   (b) MT localization
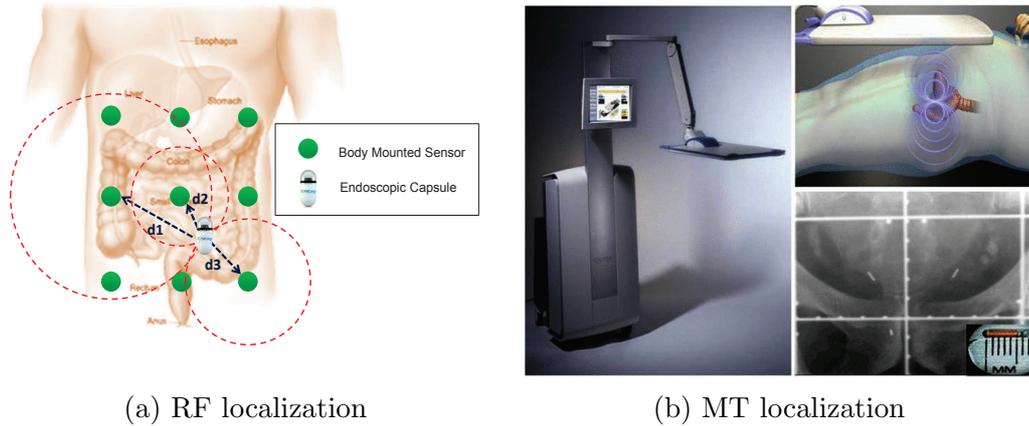
Figure 1.2: Traditional localization techniques include RF localization (a) and MT localization (b). RF localization technique uses several sensors to detect the signals transmitted from the video capsule and estimates the most likely position of the video capsule, while MT localization technique uses the similar idea to use a sensor array to detect the electromagnetic field properties.

frequency (RF) based technique [25] and magnetic tracing (MT) based technique.

Since the video capsule continuously transmits RF signal toward outside the human body, the characteristics of the signal can be analyzed and utilized to allocate the signal to a specific location [26] [27]. The basic ideas of the RF localization technique are very similar to Global Positioning Systems (GPS) [28], as shown in Figure 1.2a. To be specific, a bunch of body mounted sensors are attached to the anterior abdominal wall to detect the ultra-high frequency (UHF) band signal emitted from the video capsule [1] [29] [30]. The received signal strength (RSS) [31] [32], time of arrival (ToA) [33] [34] [35] and phase of arrival (FoA) [36] are used to measure the distance from each sensor to the video capsule. Given ranging estimates from three or more different sensors, the location of the video capsule is estimated by pattern matching algorithms such as the last square algorithm [37] and the maximum likelihood algorithm [38]. The biggest problem with RF localization comes due to the non-homogeneity of the body medium. The features of the received signals are poorly correlated with the distance, which results in discontinuous and scattered estimation with unacceptable amount of error.

Another alternative for locating the video capsule inside the small intestine is to use MT based technique [39], as shown in Figure 1.2b. As human body has a magnetic permeability very close to nonferromagnetic material such as air and water, and exerts very little influence on the static magnetic field, it is possible to achieve high tracing accuracy [40] [41]. First a magnet is attached inside the video capsule and multiple magnetic sensors are set outside. As the magnet moves, it establishes around the human body a static magnetic field. The intensity of the field is related to the magnet's three-dimensional (3D) location and 2D orientation. Thus at least five sensors are required to provide the field intensity to solve five simultaneous equations. The advantage of this technique is that it can provide both location and orientation of the video capsule which is convenient for potential use such as to control the orientation of the capsule by external electromagnetic equipment [42]. The disadvantage of this technique is that it needs a special video capsule equipped.

To conquer the problems with RF localization technique and MT localization technique, a third way to locate the video capsule during its transition, visual based motion tracking of VCE (as shown in Figure 1.3), has been discussed during the past a few years and opened up a new world of in-body localization [43] [44] [45].

Figure 1.4 illustrates the basic procedure of visual based motion tracking method. The video capsule takes images in a certain time interval (e.g. 1 shot/half second). The majority of the content in endoscopic images is the projection of the walls of small intestine, which can be assumed still during the capsule taking two adjacent frames, because averagely the displacement of the capsule during the time interval between two adjacent frames is only $0.3mm$. Many of the points in one frame can be detected in the next adjacent frame even after geometric distortion and illuminative variations. Each of those points is referred as a feature point (FP) and there have been a few algorithms for FP detection such as affine scale invariant feature transform (Affine SIFT or ASIFT) [46] [47] which will be introduced in section 5.1, and speed up robust features (SURF) [48].

After detecting the FPs in the endoscopic images, the displacement of each

17

FP is calculated. According to perspective projection transformation, as for each FP, its displacement shown in the images is the actually the projection of its real displacement in the 3D world. And because the small intestine is assumed still, it is the capsule's motion that causes the displacement of the FP and since the capsule's motion and the intestine walls' motion is relative, the displacement of the FP in 3D world can reflect the displacement of the capsule. Thus, given a starting point, integrating the displacement, which is also called motion vector, of the capsule over the time will generate the whole motion path. Because each two adjacent frames are correlated to a specific small segment (motion vector) of the path, once an abnormality is found in the video source, the location of the capsule which is the location of the abnormality can be easily achieved after finding the its position in the time axis. There are two big advantages of this technique, first of which is that it doesn't require any extra devices. The video itself is the only source that is needed, which is extremely patient-friendly. The second advantage is that is technique is very sensitive to the local change in location. The location of the capsule at each point of time is calculated by adding a motion vector to its previous location, which means there will never be a big change in location between

(b) Endoscopy images

(a) A video capsule examines the small intestine

(c) Reconstructed motion path
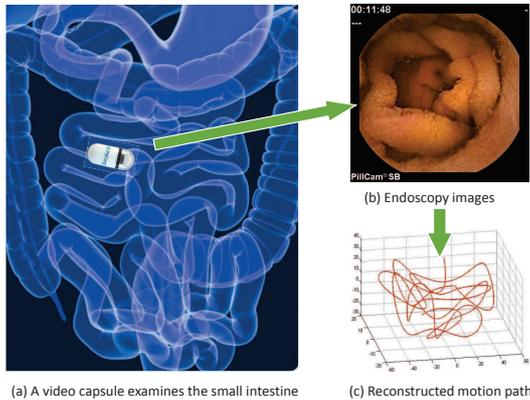
Figure 1.3: visual based localization technique uses the video source itself to track the motion of the capsule and generate the path as the video capsule transits in the small intestine.
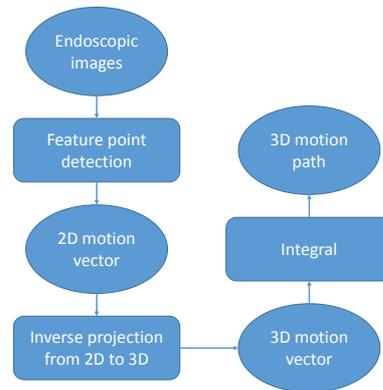
Figure 1.4: The procedure of visual based motion tracking method. The basic idea to the reconstruct the motion path of the capsule and correlate each frame to a specific location in the path.

18

two adjacent points of time. The second feature of motion tracking technique also causes its biggest disadvantage. Since the state of the capsule is related and is only related to the previous result (which is like Markov chain), every piece of error in every calculation will accumulate as the calculation continues, while in RF and MT localization, the estimates are completely independent to each other at every point of time. To conquer this problem, researchers have been studying on a hybrid solution combining RF and motion tracking methods to provide the estimates [43] [49].

1.3 Motivation

In-body localization techniques face one of their biggest challenges when conducting experiments for validation of themselves [50]. To validate these methods, the ground truth which in this case is the real location of the video capsule in the small intestine, must be known. However, once the video capsule is ingested by a patient and passes through the GI tract, there is no mechanism to control the capsule's speed or direction as it traverses the GI tract [51]. It is also particularly difficult to measure the capsule's location or orientation during its traversal within the human body. This means that the capsule must be somehow visible during its transition. Thus during the experiment, either the location of the capsule is obtained by other convinced means such as X-ray or the location is obtained surgically, both of which are impractical and illegal in the United States whether the experiments are carried out on human beings or animals. Thus it becomes necessary to build a testbed containing a small intestine model and a video capsule for validating localization algorithms and yet there has not been any article discussing about how to build such a testbed.

Unlike other testbeds for RF or MT localization or for micro-robotics control, a subtle change on the shape of the model could make a big difference on the motion tracking results, because the motion tracking algorithms are extremely sensitive to micro changes in consecutive pictures. However, it is extremely difficult to find a

material to imitate the walls of small intestine which has twisted shape and good elasticity and at the same time the walls of small intestine can be completely fixed during the experiment. Even if such a kind of material or even a piece of excised porcine small intestine specimens is found and applied in the testbed, there is no way to precisely simulate the motion of the capsule as it is pushed by intestinal peristalsis.

An alternative way to emulate the procedure of video capsule endoscopy is to use a virtual testbed in which a virtual camera travels along a virtual 3D small intestine model and generates emulated endoscopic pictures. There are plenty of articles talking about virtual testbeds to emulate small intestine in the literature, but none of them is designed for localization of VCE. When designing a testbed for localization, the essential part during the emulation is that each emulated picture should be correlated to a specific location where the virtual camera is when taking the picture. In this way, other researchers can apply their algorithms on those pictures, obtain their own estimates of the location of the camera and compare their results with the location provided by the testbed.

1.4 Contribution

In this thesis, three aspects of a virtual testbed for visual localization experiments inside the small intestine is introduced in three aspects. First the setup procedures and visual interior and exterior appearances are described in details. Then in order to validate that the virtual testbed works as a real physical testbed, based on a sequence of pictures provided by the testbed, the location of some selected points are tracked on the pictures and compared with theoretical values. At last, based on the testbed, three typical situations - straight, bent, contraction - are emulated respectively. The motion tracking algorithms are extremely sensitive to the radius of the small intestine and contraction unpredictably changes the radius. Thus a geometric model for estimating the radius of the small intestine is given to assist

researchers to make their algorithms adjustable to these dynamical changes. Empirical results have shown that the proposed virtual testbed can provide realistic emulated endoscopic images for visual based localization algorithms such as motion tracking.

The major contribution of this thesis is that it provides an alternative way to validate visual based localization algorithms. Although there have been many attempts to build virtual testbeds for experimentation, few efforts have been made for application of localization. The special point of building a testbed for localization is to set the scenarios friendly to the localization algorithms. For example the cross section of the small intestine model must be a perfect circle; the motion path of the virtual camera must be in the central axis of the model; and the most important thing is that each emulated picture must be correlated to a specific location in the motion path so that the researchers can compare their results with the location provided by the testbed. The proposed testbed is designed to meet these restrictions, which fills the hole in the field of validation of visual based localization algorithms.

The other main contribution of this thesis is that it brings up an issue of the influence of contraction on visual based localization algorithms. Because the algorithms are extremely sensitive to the radius of the small intestine, usually researchers would assume the radius to be constant to simplify the scenarios. But in reality, the size of the small intestine is changing dynamically. Because VCE doesn't involve any other devices' assistant, it is desirable to measure the size of the small intestine from the video frames in order to make the localization algorithms to be more robust. In this thesis, a geometric model for estimating the size of the small intestine during contraction is discussed and tested using the virtual testbed. The results are fairly accurate.

Besides, the testbed provides a way for researchers to compare their methods with each other because if different methods use different datasets for validation, it is not convincing to differentiate the accuracy or other metrics of the results. Using the same video source from the virtual testbed, all different methods can compare

their results with the same values provided by the testbed.

The thesis draws substantially from results presented previously in:

1. Mi, Liang, Guanqun Bao, and Kaveh Pahlavan. "Design and validation of a virtual environment for experimentation inside the small intestine", In Proceedings of the 8th International Conference on Body Area Networks, pp. 35-40. ICST (Institute for Computer Sciences, Social-Informatics and Telecommunications Engineering), 2013.

2. Mi, Liang, Guanqun Bao, and Kaveh Pahlavan. "Geometric Estimation of Intestinal Contraction for Motion Tracking of Video Capsule Endoscope", In Proceedings of SPIE Volume 9036, Medical Imaging 2014: Image-Guided Procedures, Robotic Interventions, and Modeling, San Diego, 2014.

3. Bao, Guanqun, Liang Mi, and Kaveh Pahlavan. "Emulation on motion tracking of endoscopic capsule inside small intestine." In 14th International Conference on Bioinformatics and Computational Biology, Las Vegas. 2013.

1.5   Outline

The thesis is organized as follows:

Chapter 1 gives an brief introduction of the evolution of VCE, several localization techniques for VCE as well as motivation and contribution of this thesis. chapter 2 focuses on the background of visual based localization of VCE and visual emulation of the procedure of VCE inside small intestine. chapter 3 presents the procedure and related techniques for designing testbed for validating visual based localization algorithms. In chapter 4, intestinal contraction are emulated using the virtual testbed, and a geometric model for measurement of intestinal contraction is introduced and tested with the virtual testbed. A series of experiments on speed estimation of video capsule are described in chapter 5. One groups of experiments

focuses on straight tube while the other focuses on contracted tube. Speed estimation involves inverse transformation from 2D space to 3D space, which is also covered in the chapter. Finally conclusions and suggestions of future work of this research are presented in chapter 6.

Chapter 2

Background in Visual Based Localization and Environment Emulation of Small Intestine

This chapter includes a background review of related methods that are related to this thesis. Section 2.1 talks about the background of visual based localization technique. Section 2.2 talks about the testbed of VCE and especially emulation of the inside environment of small intestine for the use of motion tracking.

2.1 Background in Visual Based Localization of VCE using Video Source

VCE [52] provides a means to obtain a detailed video source of the inside small intestine. In 2001, VCE became available for the evaluation of patients with probable small intestinal hemorrhage [53]. Advantages of VCE include that the procedure is noninvasive, requires no sedation, and does not expose the patient to ionizing radiation. The major limitations of the capsule endoscopy were its inability to obtain a biopsy, precisely localize a lesion, or perform therapeutic endoscopy. The

advent of the VCE has released the endoscopist from the requirement to exert force on a long floppy cable-type endoscope to examine relatively short segments of small intestine. A two-dimensional to three-dimensional mapping of the VCE images is proposed as well as the alignment of the consecutive images [54]. It resolves a very serious limitation of the inverse projection of VCE images by detecting the angle of the VCE so as to realize the alignment of the center of the small bowel.

In literature [55], the researchers focus on the development of a virtual reality - based trainer for colon cancer removal. It enables the surgeons to interactively view and manipulate the concerned virtual organs as during a real surgery. Literature [56] proposes a new approach to simulate the small intestine in a context of laparoscopic surgery. The aim of this work is to simulate the training of a basic surgical gesture in real-time: moving aside the intestine to reach hidden areas of the abdomen. This paper uses a layered model to animate the intestine. The intestine's axis is animated as a linear mechanical component.

[21] describes a method for tracking the motion of a real endoscope by epipolar geometry analysis and image-based registration. In an endoscope navigation system, which provides navigation information to a medical doctor during an endoscopic examination, tracking the camera motion of the endoscopic camera is one of the fundamental functions. [57] presents a frontier-work on the registration of real and virtual endoscopic images. It uses branching structure information of the bronchi. [58] describes a method for tracking the motion of a flexible endoscope, in particular a bronchoscope, using epipolar geometry analysis and intensity-based image registration. It tracks camera motion using real endoscopic video images obtained at the time of the procedure and X-ray CT images acquired before the endoscopic examination. A virtual endoscope system is used for generating virtual endoscopic images. The basic idea of this tracking method is to find the viewpoint and view direction of the VCE that maximizes a similarity measure between the virtual and real endoscopic images. [59] describes the Karlsruhe Training System for Endoscopic Surgery. The most important features of the system are geometrical

and kinematical modeling, a hierarchical data concept, multibody-dynamics, and support of haptic devices, multiple levels of details, various rendering modes and stereo-viewing.

In [60], the Model of Deformable Rings (MDR) is developed to pre-process WCE video and aid clinicians with its interpretation. The MDR uses a simplified model of a capsule's motion to flexibly match (register) consecutive video frames. It computes motion-descriptive characteristics and produces a two-dimensional representation of the GI tract's internal surface - a map. The authors also indicate that an analytical torque model is proposed and subsequently validated. The proposed torque model can be used in the design and optimization of in-body robotic systems, which can remotely be articulated using magnetic actuation. [61] models the current prototype tip, named EDORA. The model is a "tube" of about 1.5 m in length, starting at the caecum and ending at the rectum. Some of the curves of the intestine are very difficult to operate with the current colonoscopies. The operation of colonoscope is a very technically demanding endoscopic examination and makes patients uncomfortable.

2.2 Testbed for VCE

There have been a few attempts to emulate the human intestine either physically and virtually.

2.2.1 Physical Testbed

In [62], the authors build a physical testbed with a piece of porcine large intestine 150 cm long and 6 cm in diameter. Some markers are attached inside the intestine for detecting the change of diameter of the intestine. A flexible endoscope is placed to simulate the view from a capsule endoscope. The exterior and interior appearances are shown in Figure 2.1.

Another research group [63] also use a piece of real porcine colon specimens to setup a testbed for ex vivo experiments on the locomotion of a micro-robot capsule, as shown in Figure 2.2.

Some other similar ex vivo experiments using physical intestine model [The International Journal of Robotics Research]

In [64], the authors immerse a plastic tube into oil in order to simulate the environment of GI tract for testing their proposed capsule-robot.

2.2.2 Virtual Testbed

Virtual testbed for emulation the small intestine has been discussed for a few decades, as the development of 3D computer graphics techniques [65].

In [50], a realistic 3D virtual model is introduced as shown in Figure 2.3. The model is built by creating a cylindrical tube along a path, with a varying diameter. Then the researchers add mechanical reaction to the surface of the model such that when the user touch it, the shape will change according to the mechanics principles.

After stepping into the 21st century, there have been a trend to conduct virtual

(a) RF localization   (b) MT localization
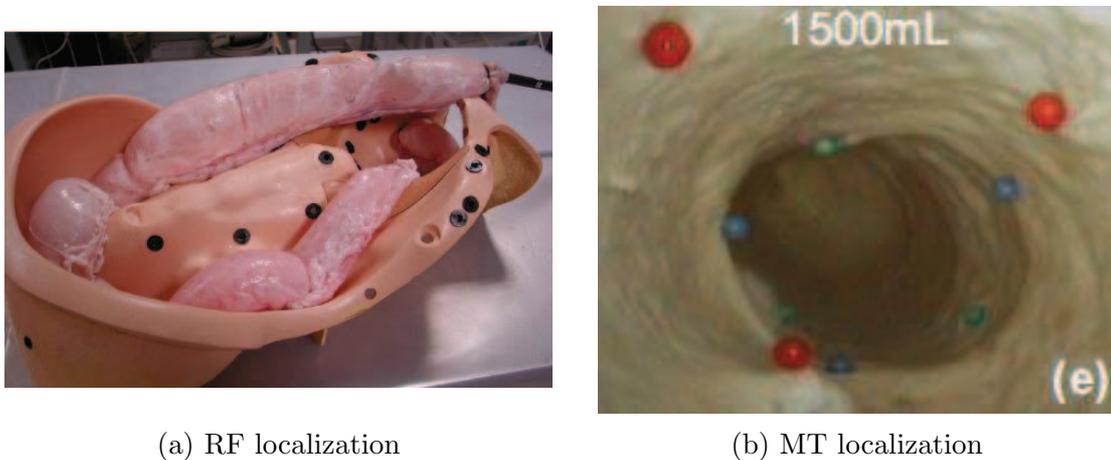
Figure 2.1: The exterior and interior appearances of the environment for insufflation into large intestine. Ex vivo porcine intestine is arranged in a phantom model to simulate the shape of the human colon within the abdomen. When the intestine is inflated with 1500 mL air, the markers attached on the internal surface are exposed to the camera.

Figure 2.2: The exterior and interior appearances of the environment for experiments on the locomotion of a micro-robot capsule.

endoscopy (VE) based on the CT datasets . Based on the results from CT scan, researchers have been able to reconstruct a 3D model of human organs and set a virtual camera to travel inside the organs. Some early publications talking about this technique can be found in [66] [67]

In [68], the authors use face rendering techniques to generate the scenes of the inside of the stomach from the CT datasets and compare the reconstructed virtual model with the clinical results from the view of a gastric fiberscopy (GF).

(a)   (b)
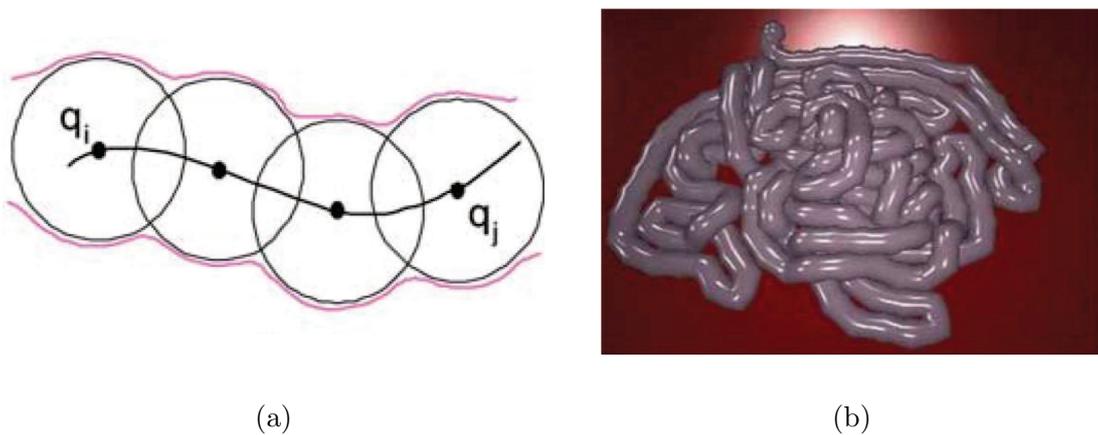
Figure 2.3: A virtual model of small intestine for virtual surgery. The shape of the small intestine is defined by a bunch of spheres whose centers are on a specific path.
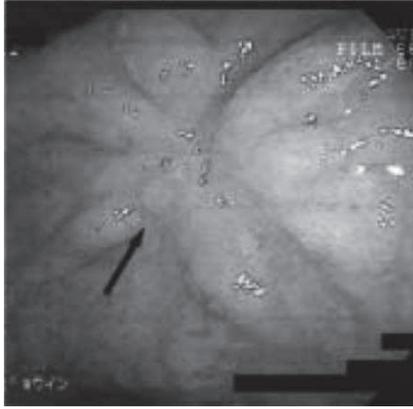
(a) VE view
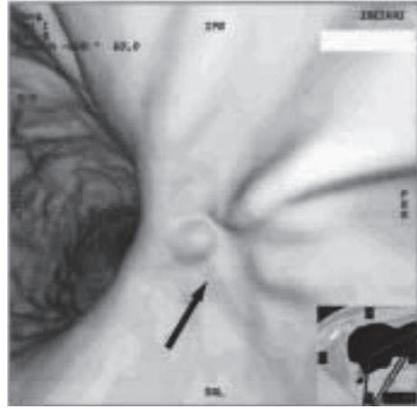
(b) GF view

Figure 2.4: Early gastric cancer, type IIc is found inside the stomach using CT-based VE and GF. A smooth elevation and convergence of mucosal folds (arrow) are seen at the antrum pylori of the stomach by (a) VE and (b) GF.

In [69], a colon phantom is produced using 3D printing (MakerBot) from a stereolithography model generated from real Computer Tomography Colonography (CTC) data of a 25 cm long section of transverse colon with two polyps.

Piotr Szczypinski and his research group have developed a speed estimation algorithm for the VCE and introduce their experiments in a virtual environment of small intestine in [60] and mentions the virtual testbed used for validation as shown in Figure 2.6. But still, they use the images produced by the testbed without validating the testbed.
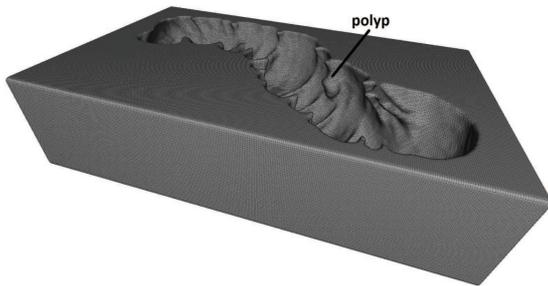
(a) Underlying 3D stereolithography model for 3D-printing a colon phantom.

(b) A colon phantom is painted after 3D-printing in order to mimic the visual features of colonic mucosa

Figure 2.5: A physical model to emulate human colon by using 3D-printing technique
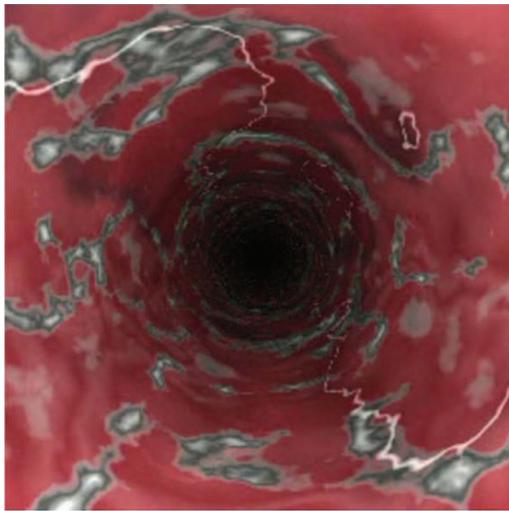
Figure 2.6: An emulated endoscopic image for validating speed estimation of video capsule endoscope.

Chapter 3

Design of a Testbed for Experimentation of Visual Based Localization in Small Intestine

It is very difficult to verify the performance of an motion tracking algorithms inside small intestine, because doing experiments on human body is extremely costly and restricted by law, and because of the limitation of the control of the capsule. Thus a testbed becomes practically useful for algorithm validation.

Generally there are two options for testbeds. One option is to build a physical testbed and the other is to build a virtual testbed. Both kinds of testbeds are implemented in this research. Figure 3.1 compares the interior and exterior appearances of physical testbed, virtual testbed and real small intestine.

This chapter discusses the setup procedure and the features of physical testbed and virtual testbed. As part of our conclusion, the virtual testbed is considered more practical than the physical testbed with respect to validation of motion tracking algorithms. Validation methods of our testbed are also presented in this chapter.
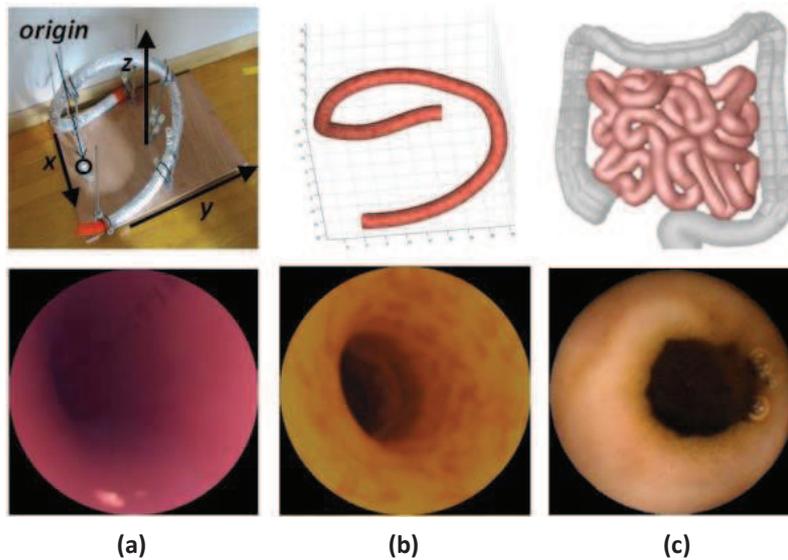
Figure 3.1: Comparison among physical testbed (a), virtual testbed (b) and real small intestine (c). three upper pictures show the exterior appearances while three lower pictures are the corresponding interior looks.

3.1 Design of a Physical Testbed

Clinical data show that the average length of a human small intestine is 7-9 meters long and the capsule stays in the small intestine for about 3-4 hours. If the capsule is assumed to travel at a constant speed, then the average step distance between two consecutive frames can be roughly calculated as 0.03 cm. During the few hours when the capsule is in the small intestine, it takes pictures at a constant rate. According to literatures and the product specifications, the rate is commonly 2 frames per second due to limited energy. Some capsules can support 3 frames per second and even up to 6 frames per second [70]. In this research, the rate is assumed 2 frames per second.

To simulate the transition of the video capsule, a wired endoscopy camera equipped with four LED is used and inserted into the tube with a approximate constant step of 0.03 cm. In the endoscopic pictures, the tube surface that lied physically closer to the camera has a brighter intensity value. The brightness de-

creases as the distance increases and finally at the far end of the tube, which is corresponding to the center of the endoscopic pictures, a black hole will form. If the camera is about to tilt, the black hole would move toward to the edge of the endoscopic pictures. Figure 3.1a indicates a test picture take from inside the physical testbed. We can see that it is extremely similar with real pictures taken from small intestine as shown in Figure 3.1.

To simulate the structure of human small intestine with a mechanic model in an acceptable size is extremely difficult, even impossible, because of many reasons. The first reason is that it is extremely difficult to find a kind of material to emulate a mechanic model with twisted shape like human small intestine. The materials of real human small intestine allow itself to bend into all kinds of shapes and at the same time to maintain its toughness. Second, the motion tracking algorithms are sensitive to even a tiny change on the surface of the model, thus the material must be non-flexible. If not, pushing the camera along the model will change the shape of the model.

Some of the physical testbed for emulation of small intestine of colon mentioned in chapter 2.2 are created using real porcine colon specimens. However, there is no way to fix the model so that the procedure of endoscopy doesn't make changes to shape of the model. Moreover, another restriction of motion tracking algorithms is that the cross section of the small intestine model must be a perfect circle. Therefore using the real porcine specimens is not practical in this research.

Several kinds of materials have been tried for emulation of small intestine and finally a piece of Polyvinyl chloride (PVC) clear vinyl tubing is used. The PVC pipe is 1.5 meter long 3 centimeter diametrical. It is bended and twisted to emulate a 3D environment for endoscopy in order to test the accuracy of the motion algorithms in any direction.

The internal and external surfaces of the tube are painted orange to make it realistic. Figure 3.2 shows the appearances of the physical model from three views. After that, the tube is wrapped with a layer of tinfoil paper to prevent the light

(a) Upper view   (b) Side view   (c) Side view
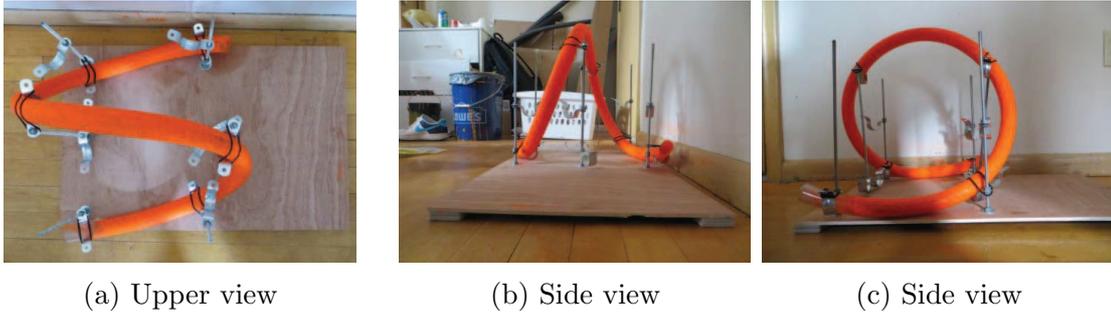
Figure 3.2: Physical intestine model from three views. The external surface is painted orange to emulate the color of the small intestine.

source from outside environment affecting the experiments, as shown in Figure 3.3

After building the physical intestine model, the remaining task is to simulate the transition of the video capsule [65]. Due to the restriction of the motion tracking algorithms, the camera must travel along the central axis of the tube so that the distance from the camera to the walls of the tube is the same in any direction. In order to implement this, the camera is tactfully fixed inside a smaller PVC tube whose external diameter is exactly the same as the internal diameter of the physical model (as shown in Figure 3.4) so that the camera can travel along the model and doesn't shake during the procedure.

The features and properties of the camera used for physical testbed are shown in Table 3.1.

The camera continuously takes pictures at a rate of 30 frames per second. Thus

(a) Upper view   (b) Side view   (c) Side view
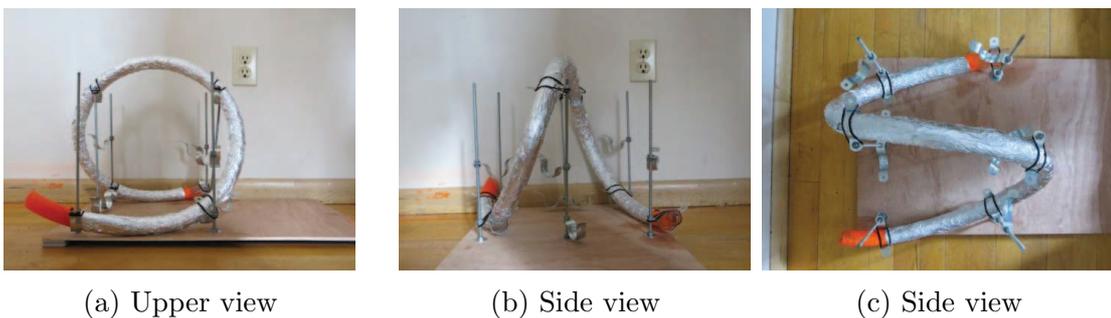
Figure 3.3: Physical intestine model from three views. A layer of tin-foil is wrapped around the model to prevent the light source from outside affecting the experiments.

(a)　　　　　　　　(b)　　　　　　　　(c)
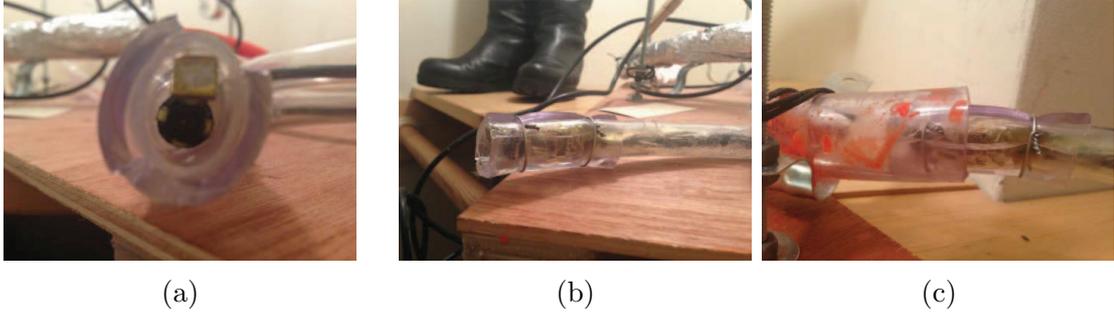
Figure 3.4: The camera is fastened inside the smaller pipe; and the smaller pipe can be pushed to move inside the physical model; lubricant is used to smooth the movement.

our testbed can provide emulated endoscopic images with different frame rate according to different requirement. Two examples of emulated endoscopic images are shown in Figure 3.5.

One advantage of the physical testbed is that it is intuitive. It provides realistic endoscopic images for post-processing. Another big advantage is that physical model can be immersed into liquid in order to simulate the external environment of the small intestine, especially the electromagnetic environment.In this way, the propagation characteristic of wireless BAN (WBAN) channel [34] can be measured and the RF localization techniques can be employed in the testbed so that the testbed

Table 3.1: Features of the camera used in the physical testbed

Feature	Description
Waterproof level	IP 67
Sensor	1/6 CMOS Image Sensor
Angle of view	62°
Resolution	$640 \times 480 \ pixel^2$
Head outer diameter	14.5 mm
Data cable length	5 m
Frame Rate	30 fps

Figure 3.5: Two example pictures from the physical model; the pictures indicate the capsule is going to turn left if it is moving forward

can validate the hybrid localization algorithms combining visual-based techniques and RF techniques [43].

However, there are still several drawbacks of a physical testbed:

- A big drawback is its restriction in camera control. After the camera is inserted into the tube, the only possible movement of the camera is along the tube with linear proceeding distance, rather than tilt and rotation. Although the motion tracking algorithms doesn't require the camera to tilt and rotate, to simulate controllable rotation and tilting are also useful to validate the robustness of the algorithms.

- Besides, to emulate the complicated shape (especially the sharp turn) of the small intestine is very difficult because there is barely a kind of materials that can be as smooth and soft as small intestine and similar toughness at the same time. And the camera would get stuck at the corner.

- Plus, adding texture on the physical model to make it exactly the same as small intestine is also unpractical.

An alternative way to solve the programs listed above to use 3D printing techniques to build a physical model of small intestine exactly according the require-

36

ments. And yet this may dramatically increase the expense of the research and involve legal issues [71] [72] [73]. Actually using CT to scan the small intestine, reconstruct the 3D virtual model and then using 3D printing technique to reconstruct the physical 3D model has becoming a promising area in testbed design for VCE [69].

Besides using a physical testbed for validation of motion tracking algorithms, another solution is creating a virtual 3D model of small intestine and simulating a virtual camera to travel along the inside of the model. In the next section, a detailed discussion of virtual testbed is presented.

3.2   Design of a Virtual Testbed

Although the physical testbed cannot provide usable emulated images, it still can be considered as a reference to justify the virtual testbed, because its interior appearance are extremely similar with that of real small intestine. Thus the physical testbed serves as the model to build a virtual. Measuring the physical testbed would be the first step and then a virtual model of small intestine that shares the same shape with the physical model is created. After that a piece of texture that is extracted from real porcine small intestine is attached to the virtual model. Next steps are to generate the emulated endoscopic images on the screen This involves perspective projection and illumination effect, which will be introduced respectively below.

3.2.1   Creating 3D Virtual Model

The first step is the measure the physical model. To measure the physical model, a Cartesian coordinates systems is set to define the coordinates of every point of the model. The origin is set as the foot of a pillar and it is assumed that three orthogonal axes as x axis, y axis, and z axis respectively, as shown in Figure 3.1.

Second, the coordinates of the external surface of the model are sampled and mapped to computer. Using curve fitting and Interpolation to the surface, the skeleton of the model is then estimated as shown in 3.6a. Because of the restriction of motion tracking algorithms, the cross sections of the model have to been assumed perfect circle. Thus basically the virtual model is built by creating a piece of cylindrical tube around the skeleton, as shown in 3.6b. The tube is made up of 16167 cylinders with the same certain radius.

Moreover, the virtual model of the entire small intestine is also emulated using the similar procedure, implemented with both Matlab and OpenGL. 3D mesh data is obtained from [74]. The emulation results are as shown in Figure 3.7. The results have been used in [43].

3.2.2 Creating 2D Projection of 3D Model to a View Point

There are several ways to emulate virtual VCE such as using software like 3D Max, or by programming with Matlab and OpenGL. Compared with others, using OpenGL has its biggest advantage of flexibility. To track the motion of the capsule, it is desirable to be aware of the parameters of the testbed such as the location of each
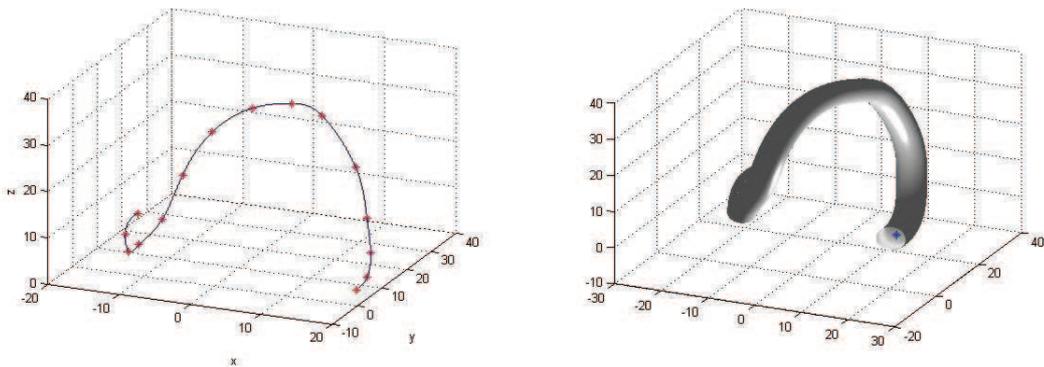
(a) Skeleton of the physical model is extracted and mapped to a virtual 3D space.

(b) A cylindrical tube is created around the skeleton to form the surface of the model of small intestine.

Figure 3.6: Mapping physical model into computer and creating a corresponding virtual model.
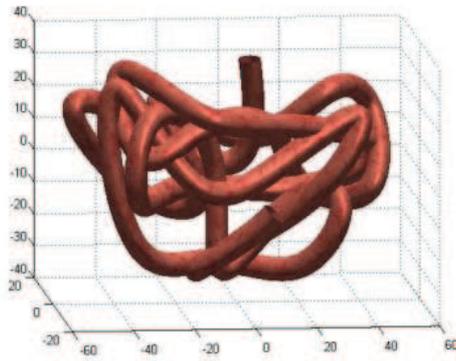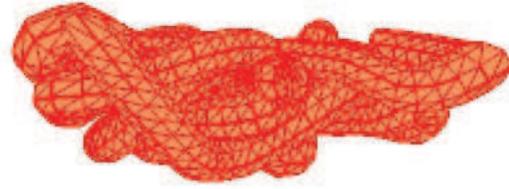
(a) Matlab   (b) OpenGL

Figure 3.7: Virtual model of entire small intestine implemented with Matlab and OpenGL. First the original mesh is shrunk toward its central axis to generate a path along the structure, and then the virtual model is created by building tremendous amount of small cylinders along the path and finally Matlab and OpenGL are used to render the model.

point of the model mesh, the normal vector of each surface, the lighting properties (ambient, diffuse, specular) of interior walls of small intestine as well as the light source and at last but not least the projection matrix. By using OpenGL (and other libraries for example Direct3D), it is possible to properly set those parameters as needed.

First a cylindrical tube with a certain radius is created. In our case, a straight and bend tube is created respectively for the use of studying the relation between the BH and the intestinal contraction as well as the relation between the BH and the bend of small intestine. A uniform color is mapped inside the tube because complex texture can bring influence on the measure of the size of shape of the BH. A virtual camera is set on the axis of the tube, which is regarded as the motion path of the camera. The direction of the camera is set to face forward to the next point on the axis. A spot "Phong" light source is then added at the same location with the camera face the target of the camera and it moved at the same speed and direction with the camera. In order to simulate the LEDs equipped in the front of the capsule, the angle of the spot light is set very large so that it can lighten all

39

the areas that would appear in the simulated video. After the testbed is setup, it is necessary to do projection transformation from 3D to 2D in order to obtain the emulated endoscopic images shown on the screen.

Commonly used transformation method to generate the projection of 3D object to a 2D plane is perspective projection [75], because it simulates the projection mechanism of human visual system. Equation (3.1) demonstrates the transformation matrix:

$$
A = \begin{bmatrix}
\frac{2N}{x_{max}-x_{min}} & 0 & \frac{x_{max}+x_{min}}{x_{max}-x_{min}} & 0 \\
0 & \frac{2N}{y_{max}-y_{min}} & \frac{y_{max}+y_{min}}{y_{max}-y_{min}} & 0 \\
0 & 0 & \frac{-(F+N)}{F-N} & \frac{-2FN}{F-N} \\
0 & 0 & -1 & 0
\end{bmatrix},
\tag{3.1}
$$

where x_{min} and x_{max} indicate the left and right boundaries of the near plane, y_{min} and $y_{m}ax$ restrict the bottom and top edges of the near plane, while $N = z_{near}$, $F = z_{far}$ indicate the z values of near and far planes, as shown in Figure 3.8.

The matrix is applied on each of the point of the model as shown in Equation 3.2.

$$
\begin{bmatrix}
X_i \\
Y_i \\
Z_i \\
1
\end{bmatrix}
= A
\begin{bmatrix}
x_i \\
y_i \\
z_i \\
1
\end{bmatrix},
\tag{3.2}
$$

where $\begin{bmatrix} x_i & y_i & z_i & 1 \end{bmatrix}^T$ are the original coordinates of each of the test point and $\begin{bmatrix} X_i & Y_i & Z_i & 1 \end{bmatrix}^T$ indicates the location on the pictures of test points, i is the index of each point.

After transformation (most of the calculation are conducted automatically in hardware which is graphics processing unit (GPU)), every point of the mesh of the
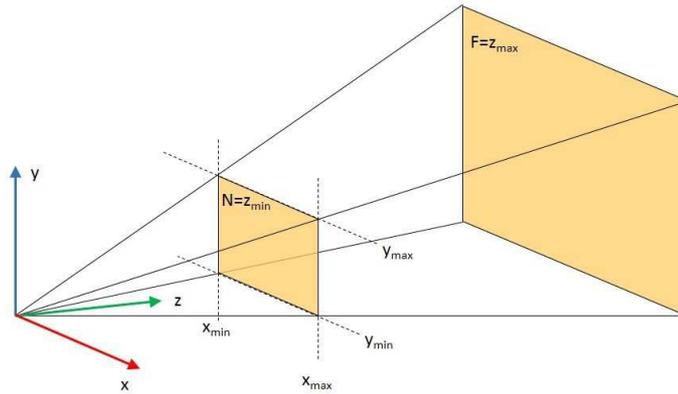
Figure 3.8: Perspective projection frustum

small intestine model is projected to a 2D screen (as shown in Figure 3.9) and if a surface is blocked by another surface, it would be automatically removed in order to reduce the amount of computation and the memory storage. It is assumed that the angle of view is 90°. Resolution of the simulated endoscopic video is set 512 x 512 $pixel^2$. As shown in the figure, brightness of the walls that are closer to the center of the picture (which means they are farther from the camera) are diminishing until to be completely black. This is because the luminance decreases exponentially as light travels through space, which will be introduced in 3.2.3. After crossing a marginal value, it is considered that no light hit the walls of small intestine and reflect toward the camera and the marginal value is specified visibility which is the maximum distance that can be seen from the camera.
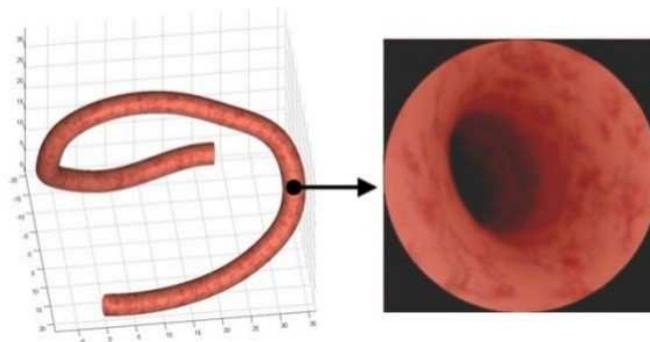
Figure 3.9: Exterior and interior appearances of the emulated small intestine

3.2.3   3D Illumination Effect

In reality, everything shown on a screen is an image with a certain resolution. No matter how we define the image, such as the projection of 3D model, eventually it is only an plane image shown on the screen. The perspective projection is a method to simulate the imaging process of human body. During the procedure of VCE, the LED in the capsule is the only light source. Given this light source, those things whose reflection light can go through the lens and hit the image sensor are the things shown on the screen. Thus the brightness of the things in the image shown on the screen totally depends on their reflection light. And the brightness are reflected as the change of the original RGB values of the pixel. Therefore, the influence of the light source is eventually reflected on the RGB values of the pixels of endoscopic images.

On one hand, different materials have different ability to reflect lights. For example given the same light source, metal tends to look more shinning than wood. In the field of computer graphics, commonly three special parameters are used to describe the lighting properties of the materials, which are ambient, diffuse, and specular [76] [77]. Each of the property has its own RGB values, such in Equation 3.3 .

$$\begin{cases} ambient_{material} = (red, green, blue) \\ diffuse_{material} = (red, green, blue) \\ specular_{material} = (red, green, blue) \end{cases} \tag{3.3}$$

On the other hand, light source has its own lighting properties of ambient, diffuse, and specular as materials which can be specified as in Equation 3.4. For example red light makes material look "more red" and so on. Multiplying the lighting properties of light source and the material gives the final lighting properties as in Equation 3.5. So the colors that are finally projected on the screen is the combination of the materials' lighting properties, light source's lighting properties

as shown in Equation 3.6

$$\begin{cases} ambient_{light} = (red, green, blue) \\ diffuse_{light} = (red, green, blue) \\ specular_{light} = (red, green, blue) \end{cases} \quad (3.4)$$

$$\begin{cases} ambient = ambient_{material} \times ambient_{light} \\ diffuse = diffuse_{material} \times diffuse_{light} \\ specular = specular_{material} \times specular_{light} \end{cases} \quad (3.5)$$

$$color = ambient + diffuse + specular \quad (3.6)$$

For this research, the light source lighting properties are set as follows:

$$\begin{cases} ambient_{light} = (0.3, 0.3, 0.3) \\ diffuse_{light} = (0.7, 0.7, 0.7) \\ specular_{light} = (0.6, 0.6, 0.6) \end{cases} \quad (3.7)$$

and those of material are set as follows:

$$\begin{cases} ambient_{material} = (0.5, 0.5, 0.5) \\ diffuse_{material} = (0.95, 0.6, 0.35) \\ specular_{material} = (0.12, 0.12, 0.12) \end{cases} \quad (3.8)$$

3.3 Validation of Virtual Testbed

Once the testbed is setup and the simulated video (consecutive frames) is obtained, it is desirable to validate it in order to convince that it worked fairly similar as a physical testbed. In order to validate our testbed, 40 test points are selected to reflect to movement of the walls of small intestine which is actually the displacement

of the virtual camera. Each 20 points are marked black and white respectively as shown in Figure3.10. To validate the testbed, the displacement of the points on the emulated images are calculated and based on that, the displacement of the virtual camera can be calculated. Comparison between the calculated displacement value and the real value can reflect the accuracy of the emulated pictures.

Given the locations of the test points and the speed of the camera, the locations of the points in the next state could be easily calculated since the motions of the test points and the camera are relative. Using the projection matrix, the locations of the test points on the screen were calculated as the theoretical values based on Equation (3.2). According to the algebraic properties of matrix operations, we have Equation (3.9).

$$
\begin{bmatrix} X_i \\ Y_i \\ Z_i \\ 1 \end{bmatrix} - \begin{bmatrix} X'_i \\ Y'_i \\ Z'_i \\ 1 \end{bmatrix} = A \left(\begin{bmatrix} x_i \\ y_i \\ z_i \\ 1 \end{bmatrix} - \begin{bmatrix} x'_i \\ y'_i \\ z'_i \\ 1 \end{bmatrix} \right),
\tag{3.9}
$$

where $\begin{bmatrix} x'_i & y'_i & z'_i & 1 \end{bmatrix}^T$ are the coordinates of each test point in the next state and $\begin{bmatrix} x'_i & y'_i & z'_i & 1 \end{bmatrix}^T$ reflects the location on the pictures of test points in the next state, i is the index of each point.

One way to validate the emulated pictures are as follows: first the 2D motion vectors (which is the segment with the direction from previous state, Figure 3.10a to the next state, Figure 3.10b) of the 40 test points are measured. Then using the inverse perspective transformation matrix, the 3D motion vectors of the test points are easily calculated. The transition of the virtual camera is linear, thus the motion vectors of the test points in 3D should be parallel to each of others and should be pointing the motion direction of the virtual camera. So next to ensure that the calculated displacement is along the motion direction of the virtual camera, the projection of all the 3D motion vectors of the testbed points are used instead.

Averaging the displacements gives the estimate of motion displacement of the walls of the small intestine. Because the motion of the walls of small intestine is relative to the motion of the virtual camera, the estimate is actually the estimate of the displacement of the virtual camera.

In this research, another way (which is similar with the other) is used to validate the emulated pictures. First the 2D motion vectors are measured in two groups – black and white. On the other hand, the theoretical values of the motion vectors are calculated using Equation (3.9). The comparison results are shown in Table 3.2, where b stands for black FPs while w represents white FPs. As we can see, the errors of displacement are extremely small, which means that our testbed is fairly valid for further application.

3.4   Summary and Discussion

Doing experiments on human body is extremely difficult because of individual differences and legal issues. Using testbeds to emulate the small intestine of human body for algorithm validation of motion tracking of VCE have demonstrated its promising future. In this chapter, two testbeds have been introduced respectively. Based on

(a) Previous state   (b) Next state
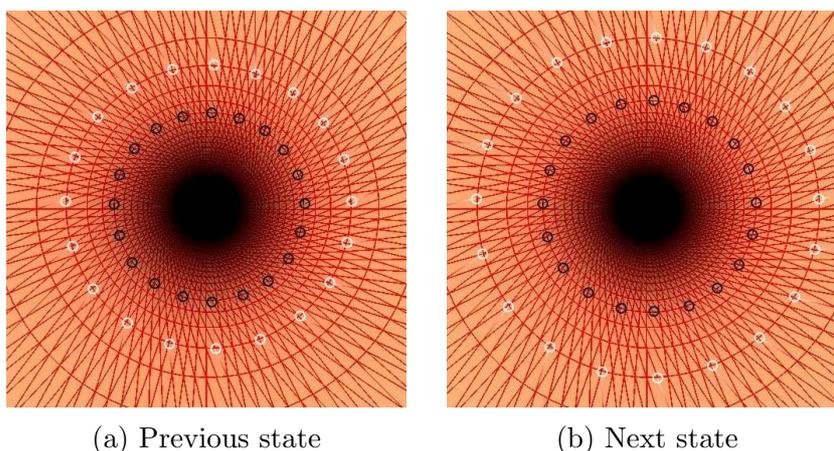
Figure 3.10: Two adjacent frames reflecting the motion of 40 FPs as virtual camera transits. From 3.10a to 3.10b, FPs are pointing outward, which means that the camera is moving forward

Table 3.2: Coordinates of test points on endoscope pictures and their comparison with estimates (theoretical values). "b" stands for black FPs while "w" represents white FPs. D denotes the displacements. Values are measured in pixels.

Tag	Xi, b	Yi, b	Xi, w	Yi, w	Xi, b	Yi, b	Xi, w	Yi, w	D, b	D, w
1	137.8	249.6	122.7	248.7	76.2	245.1	39.0	243.3	15.13	37.24
2	143.1	288.2	127.7	292.3	84.0	303.8	46.7	313.3	15.94	38.49
3	159.8	323.8	148.0	331.7	110.9	358.7	78.3	380.7	14.20	39.33
4	189.3	351.1	180.0	364.3	153.5	401.8	131.3	433.0	16.15	38.29
5	224.9	369.1	221.0	383.7	207.8	428.2	198.7	465.0	15.11	37.91
6	262.2	373.8	263.7	389.7	267.8	435.3	269.3	474.0	15.97	38.73
7	302.2	366.7	309.3	380.0	324.0	423.6	339.0	457.0	15.08	36.61
8	334.0	348.5	345.0	359.7	374.9	394.5	399.7	422.7	15.70	37.55
9	360.5	320.2	372.3	327.7	413.1	350.7	444.7	369.7	13.98	36.87
10	375.8	286.0	390.7	289.3	434.5	299.6	470.3	308.7	15.26	36.94
11	380.2	249.1	398.3	248.7	441.5	245.8	475.3	243.7	18.10	33.87
12	373.6	213.1	384.0	203.3	431.5	192.5	464.7	180.7	14.29	35.24
13	356.0	180.0	368.0	172.7	404.9	144.4	432.7	124.3	14.05	34.31
14	330.4	155.1	338.7	142.0	365.8	104.7	387.7	78.30	15.51	34.30
15	297.3	138.2	302.7	124.3	318.5	81.30	331.0	47.70	14.91	35.85
16	262.4	131.6	263.0	116.7	266.4	71.60	268.0	34.70	14.91	36.94
17	226.4	136.0	224.0	121.7	212.2	76.90	203.3	40.30	14.50	37.67
18	191.1	152.0	183.7	138.3	160.5	98.90	141.3	67.30	15.57	36.98
19	163.6	178.0	152.3	167.7	116.9	137.1	88.70	113.3	15.29	36.90
20	144.5	211.8	131.0	205.7	87.50	187.5	53.30	173.3	14.81	37.03
Ave.									15.23	36.85
Est.									15.47	36.58
Err.									1.6%	0.8%

the comparison, the virtual testbed is considered more practical for this research. A method for quantitatively validating testbed has also been discussed in this chapter. The results proved the usability of our testbed. In the next two chapters, a series of experiments using this testbed are introduced.

Chapter 4

Geometric Modeling and Measurement of Intestinal Contraction

Due to intestinal motility such as peristalsis and contraction, the shape and size of the small intestine continuously change regardless of the movement of the human body or the procedure of the VCE. The size of the small intestine, to some degree, affect the performance of motion tracking algorithm because the algorithm is very sensitive to the diameter of the small intestine, which will be discussed in details in chapter 5. Thus it is desired to study the intestinal motility as well as its influence on motion tracking algorithms.

In this chapter, emulation of intestinal contraction using the virtual testbed and measurement of the size of contracted small intestine using a geometric model is introduced. The influence of intestinal contraction on motion tracking will be mentioned is chapter 5.

This chapter is organized as follows: in section 4.1, the shape of intestinal contraction is discussed and emulation results of intestinal contraction are presented. In section 4.2, a geometric model for measuring the size which is the diameter of

the small intestine is introduced. In section 4.3, the performance evaluation of the proposed method for measuring the size of the small intestine is presented. A summary of this chapter is given in section 4.4.

4.1   Emulation of Intestinal Contraction

Clinical data shows that the average diameter of small intestine is 2-3 cm. When it is contracted, the diameter can be as small as 7 mm which is even smaller than the diameter of the wireless endoscopic capsule [78]. (Sometimes the small intestine is even closed at some place because of contraction.) The average frequency of intestinal contraction is 9-10 min^-1 consistent with localization, which means that during the several hour transition of a wireless capsule, it may come across contraction for dozens of times. Thus it is necessary to study the possible influence of contraction on the endoscopic images captured by a video capsule.

The field of view of a video capsule can be as large as 156°, so objects around the capsule, not only those in front of the capsule, take up a large space in the endoscopic images. Objects which are relatively far from the capsule have little influence on the images, including a possible contraction. In the literatures, the shape of contracted small intestine is usually assumed as shown in Figure 4.1a, compared with a piece of straight small intestine as shown in Figure 4.1b. In this research, in order to simply the situation and make it easy to do geometric modeling, it is assumed that the walls of the small intestine is stick to the cover of the video capsule when it is contracted. To be specific, the walls of the small intestine is assumed to be two pieces of cylindrical tube connected with a hemispherical tube. The cross section of the small intestine at any point is assumed to be a perfect circle due to the restriction of motion tracking algorithms [22].

Figure 4.2 illustrates the emulation results of contraction. In these two scenarios, the properties of the camera and the walls of small intestine are set the same. As shown in the pictures, the size of the BH in contracted tube (b) is much smaller than

(a) Intestinal tube is contracted.   (b) Intestinal tube is open
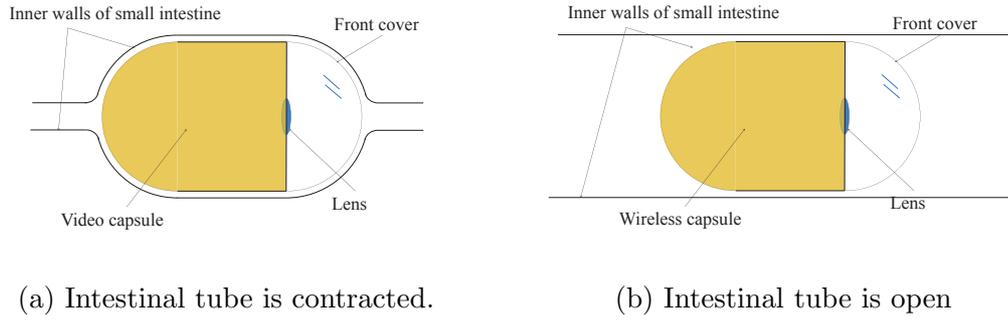
Figure 4.1: Illustration of intestinal contraction. When the small intestine is contracted, the walls of the small intestine is assumed to be two pieces of cylindrical tube connected with a hemispherical tube. The cross section of the small intestine at any point is assumed to be a perfect circle due to the restriction of motion tracking algorithms.

that in straight tube (a). Thus in order to reveal the quantitative relation between the diameter of the BH and the diameter of the contracted small intestine, fifteen models of contraction have been generated using the similar shape discussed above for comparison whose interior appearances are shown in Figure 4.3.

It is observed that the size of BH in the center of the VCE images is related to the size of the small intestine. To be specific, when the small intestine is contracted,
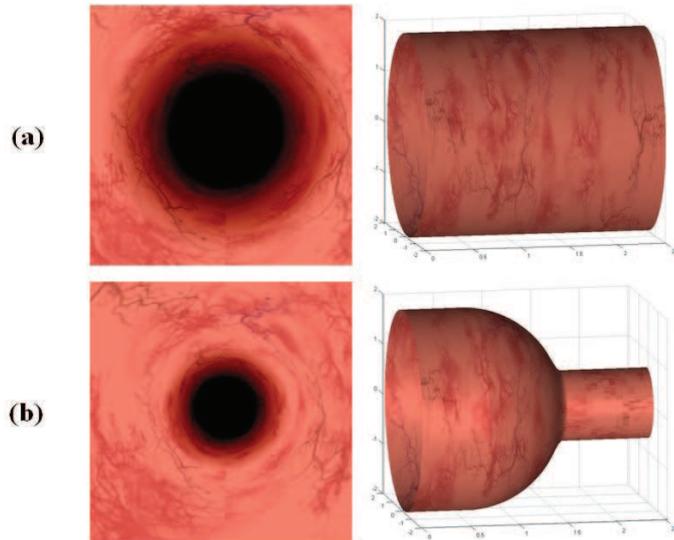
Figure 4.2: Emulation of intestinal contraction by the use of the virtual testbed.

the BH shrink into the center as the radius of the small intestine became smaller. To automatically estimate whether the small intestine is contracted and how much it is contracted from the video source, it is necessary to quantify the relation between the size of BH and the size of the small intestine. Thus we use the similar model as shown in Figure 4.2 and create 15 models that simulate the intestinal contraction with different degree. The diameter of the capsule is assumed $32mm$. The size of the BH shown in the simulated picture of each model is then measured against the radius of the contracted model (as shown in Table 4.1).

4.2 Geometric Modeling of Intestinal Contraction

In the previous section, a bunch of models of intestinal contraction have been generated for the use of quantifying the geometric relation between the diameter of the BH and the diameter of the small intestine. In this section, a geometric model for
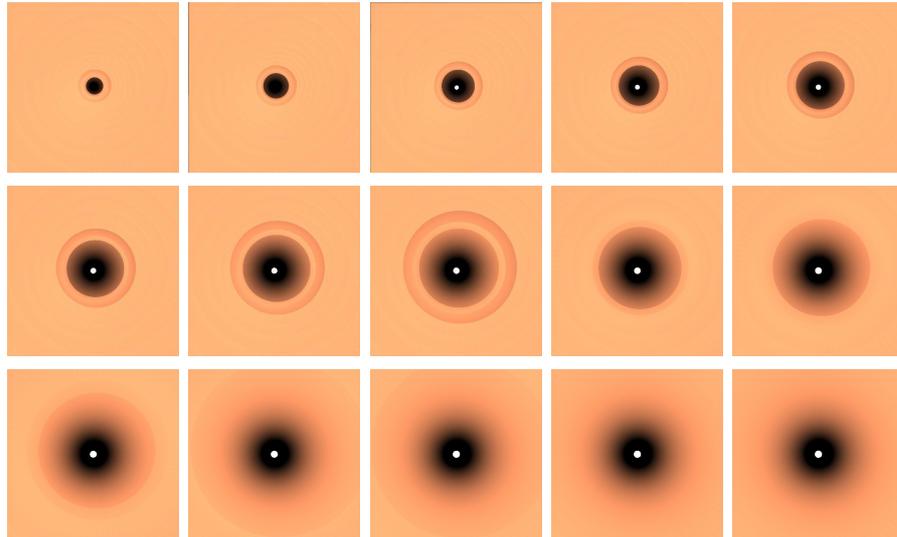
Figure 4.3: 15 emulated endoscopic images. For each of them, the small intestine is contracted with different degrees. For the fist one, the radius is 5.567 mm and for the last one, the radius is 16 mm, which is the radius of the small intestine with no contraction. Colors in these images are not continuous. This is caused by the rough surfaces and it doesn't affect the estimation results.

establishing the relation has been proposed and validated using the previous results.

Since the capsule is surrounded by walls of small intestine, these walls are projected to the 2D image plane as a bunch of circular rings [60], as shown in Figure 4.4a. Under this image acquisition systems, the points that are closer to the capsule lie on circles with a larger radius compared to the points that are farther down the intestine. As the point is getting farther away from the capsule, its brightness becomes increasingly smaller. In optics, the BeerLambert law, describes the strength of the light after it travels through a certain kind of material. The relation is specified as follows:

$$I = e^{-\alpha D_p} I_o, \tag{4.1}$$

where I_o is the light intensity at the capsule, while I is the intensity at any point p of the object; D_p is the distance from the capsule to point p; α is a parameter determined by the propagation medium, which in this case could be assumed as air or water.

According Beer's law and also it is intuitive that beyond a certain distance, there is almost no light that can be reflected back to the camera in the capsule and a black hole therefore forms. The remaining problem is whether there is a quantitative relation between the size of the BH and the size of the small intestine.

It is actually safe to assume that the "certain distance" is constant during the transition of the capsule as the certain distance is refer as visibility of the LED in the capsule. Then, as shown in Figure 4.4a, there is an imaginary plane, which acts as a boundary in front of the capsule. All the objects that are farther than the boundary are not visible to the video capsule.

In Figure 4.4a, point M lies on the closest view that can be captured by the camera. When projected on the onto the cylindrical image, M has the largest radius value r_i as shown in Figure 4.4b. Connecting M and the camera forms angle α_i which denotes the angle of view. P and Q are two boundary points of visibility,

respectively lying on the walls of straight and contracted small intestine. Their projection on the screen are P_1 and Q_1.

Considering α_s and α_c in the 3D space of inside the small intestine, it is obvious that:

$$\begin{cases} \tan\alpha_s = \frac{r_{iu}}{D_v} \\ \tan\alpha_c = \frac{r_{ic}}{D_v}, \end{cases} \qquad (4.2)$$

where r_{iu} and r_{ic} is the radius of the straight and contracted tube; D_v is the visibility from the lens of the camera to the far end. Meanwhile. Considering α_s and α_c in the triangle bounded by projection plane and the central axis results in :

$$\begin{cases} \frac{\tan\alpha_s}{r_s} = \frac{\tan\alpha_i}{r_i} \\ \frac{\tan\alpha_c}{r_c} = \frac{\tan\alpha_i}{r_i}, \end{cases} \qquad (4.3)$$

where r_s is the distance from P_1 to the center of the endoscopic image, and similarly r_c is the distance from Q_1 to the center. r_i is the size of the image which in this research is set to be 512 pixels.

(a) Horizontal view

(b) Vertical view
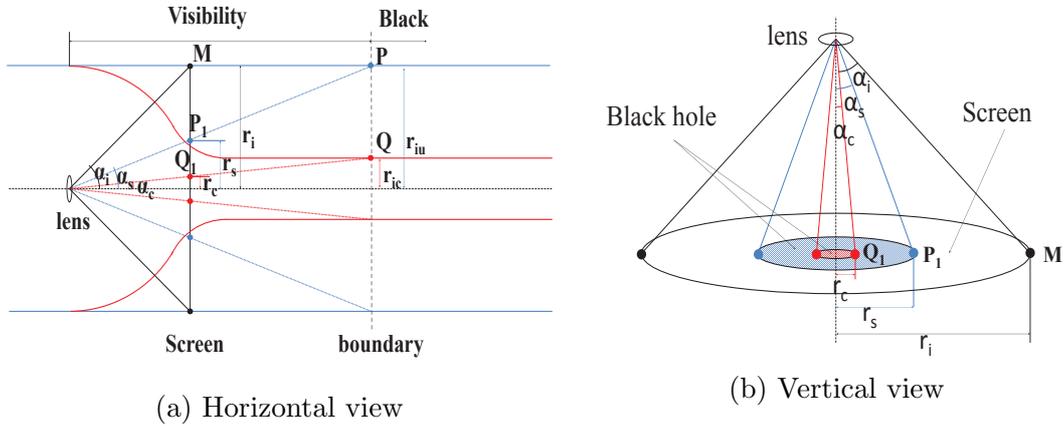
Figure 4.4: Image acquisition system. The edge of view and the edges of BHs in a straight tube (blue lines) and an contracted tube (red lines) are projected to screen respectively, forming three angles, which are used for analysis of the relation between the size of the BH and the radius of the tube.

Combining Equation 4.2 and Equation 4.3 gives the solution to calculate the radius of the small intestine as described:

$$\begin{cases} r_{is} = r_s D_v \frac{\tan \alpha_i}{r_i} \\ r_{ic} = r_c D_v \frac{\tan \alpha_i}{r_i} \,, \end{cases} \tag{4.4}$$

and consequently:

$$r_{ic} = r_c \frac{r_{is}}{r_s}. \tag{4.5}$$

According to the discussion, there are two ways to measure the size of the small intestine when it is contracted. One way is to use Equation 4.4 which involves the angle of view (α_i), the size of the image r_i, the visibility (D_v) and the radius of the BH in contracted small intestine (r_c). The other simpler way is to use Equation 4.5, but it involves the radius of the BH in straight small intestine r_s (which is usually not known before the experiment), the radius of the uncontracted small intestine r_{is} and the radius of the BH (r_c).

4.3 Measurement Results and Analysis

Based on the results from section 4.1 and section 4.1, this section talks about experiment results of measurement of intestinal contraction.

Equation 4.1 provides an estimate of the visibility. If given a lower bound of the brightness of light I_l that can be detected by human eyes, the calculated distance

$$D_l = \log(\frac{I_l}{I_o})/\alpha \tag{4.6}$$

can be considered as the visibility.

To measure the contraction, first the size of the BH in each emulated image is measured against the radius of the small intestine, as shown in the second and the third column of Table 4.1. Plug in the parameters in Equation 4.4. The estimates of

the radius of the small intestine when it is contracted is shown in the forth column. The fifth column shows the difference between the theoretical values (which are the real parameters of the model) and empirical results (which are calculated from the previous method). The comparison between analytical results and the model parameters indicates that our estimates for the radius of the model by using our geometric model matches the experiment results very well (error 6.81%). Thus given a certain average radius of the small intestine, we can easily estimate whether the small intestine is contracted and the amount of the contraction in terms of the radius of the small intestine [79].

On the other hand, it is observed that as the radius increases, the error becomes larger. This problem probably comes from the measurement of the size of the BH. In the endoscopic images, the BH is formed by decreasing brightness of the content. Thus the size of the BH is vague and can only measured based on estimation. This can be a reasonable explanation of why the errors becomes larger when the size of the BH is getting bigger.

4.4 Summary and Discussion

Physiological factors such as intestinal contraction affect the motion tracking of the VCE to a large extent. In this section, the problem of measuring the size of small intestine from the endoscopic images is addressed and a geometric model for revealing the relation between the radius of the small intestine and the radius of BH in the images is discussed. Based on the comparison of empirical and theoretical results, the geometric model is accepted as fairly valid for estimating the radius of the small intestine. Given this estimate, it is viable to detect whether the small intestine is contracted and how much it is contracted only based on the video source. Our two speed estimation algorithms provide solid results that have confirmed our expectation.

Our work would greatly benefit motion tracking for video capsule endoscope.

Table 4.1: Comparison between the real values of the radius of emulated small intestine and the estimates based on the size of black holes.

Tag	BH Size (pixel)	Radius (mm)	Estimated Radius (mm)	Error (%)
1	25	5.5678	5.43	2.47%
2	35	7.7460	7.60	1.88%
3	43.5	9.3274	9.44	1.21%
4	46	10.5830	9.98	5.60%
5	55	11.6190	11.93	2.72%
6	60.5	12.4900	13.13	5.12%
7	64.5	13.2288	14.00	5.83%
8	69.5	13.8564	15.08	8.83%
9	72	14.3875	15.62	8.57%
10	76	14.8324	16.49	11.18%
11	78	15.1987	16.93	11.39%
12	79	15.4919	17.14	10.64%
13	80	15.7162	17.36	10.46%
14	82.5	15.8745	17.90	12.76%
15	84	16.0000	18.23	13.94%
Avg.				6.81%

By using the geometric model, we are an developing an improved algorithm that is adaptive to intestinal contraction. In the future the influence of contraction will be further studied with focus on building more realistic geometric models as well as the corresponding virtual testbed by adopting clinical data.

Chapter 5

Experiments on Speed Estimation using Virtual Testbed

Speed estimation is the one of the essential parts in motion tracking (The other is orientation estimation). In this chapter, a speed estimation algorithms is introduced and reproduced. Using the speed estimation algorithms, the performance of the virtual testbed is evaluated. Moreover, the chapter also analyzes the influence of intestinal contraction on speed estimation.

Section 5.1 talks about feature point detection. Section 5.2 talks about displacement estimation of the feature point. Section 5.3 discusses the performance results of speed estimation. Section 5.4 gives the summary.

5.1 Feature Point Detection

One important step in the motion tracking is feature point detection. The basic idea of feature point detection is to detect the same point object in two different images. The purpose of feature point detection is to track the transformations such as translation, rotation, and scaling between images, which reflects the motion of the camera. It is important that the feature points extracted from the reference image can be accurately detected in the second image. According to the literature, in the

VCE application, more feature points can be detected by the affine SIFT algorithm then other algorithms [47]. Therefore affine SIFT is adopted in this research to do feature point detection.

The distance between a feature point and the capsule is very important for velocity estimation. When taking account into intestinal contraction, it is more important for researchers to understand how the contraction influences the movement of feature points in an endoscopic image. Since the capsule is surrounded by the walls of small intestine, these walls are projected to the 2-D image plane as a bunch of circular rings (Figure 5.1). Under this image acquisition system, the points that are closer to the capsule lie on circles with a larger radius compared to the points that are farther down the intestine. Therefore to better study the influence of intestinal contraction, we use basic idea of MDR algorithm to generate a bunch of rings with a certain amount of nodes in the endoscopic images, as shown in 5.2.

Every node is assigned a pair of index to, $p = 1, 2, 3, , P$, and $q = 1, 2, 3, , Q$, where p indicates the ring number and q indicates the amount of nodes in each ring. We use the following equation to transform the indexes into Cartesian coordinates:

(a) Horizontal view   (b) Vertical view
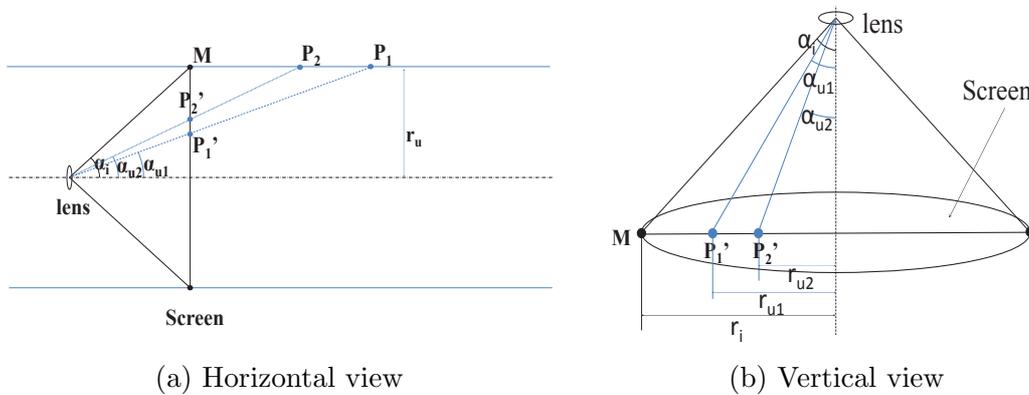
Figure 5.1: Feature point detection. M indicates the closest view that can be captured by the camera, forming the angle of view α. P_1 and P_1 refers to two feature points, forming two angular depths θ_1 and θ_2 respectively. r_u is the radius of the tube. r_{u1} and r_{u2} are the distances between P_1' and P_2' to the center of the image.

(a) Previous state   (b) Current state
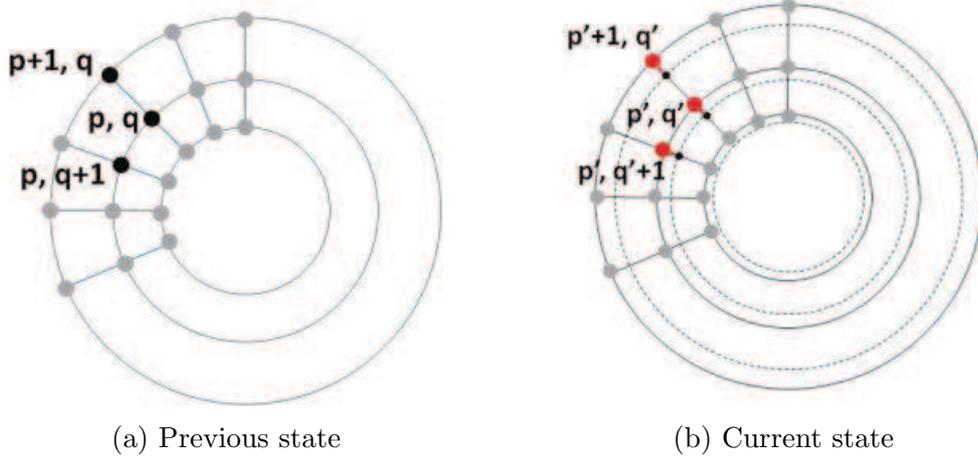
Figure 5.2: Structure of MDR. In (b), red circles reflect the structure (theoretical) in the next point of time.

$$[x_{p,q}, y_{p,q}] = rw^{p-1}[\cos \frac{2\pi q}{Q}, \sin \frac{2\pi q}{Q}] \tag{5.1}$$

where $x_{p,q}$, $y_{p,q}$, are a pair of Cartesian coordinates of a node, r is the radius of the smallest ring, w is the ratio of the radius of two adjacent rings.

Now we regard these nodes as feature points and use affine SIFT algorithm to detect the positions of the feature points in the next image. Nodes are connected as the same topology as before, as shown in Figure 5 (b). As seen in the picture, as the virtual camera move forward along the tube, all the nodes moved outward resulting in a larger radius of each ring.

5.2   Displacement Estimation

The speed of the wireless capsule can be estimated by measuring the displacement of the feature points. As shown in Figure 5.1 and Figure 5.2, feature points (nodes) that are in the same ring have the similar displacements outward if the capsule is moving straightly forward. Thus we measure the displacements of the feature points in different groups each of which consists of feature points in one ring. After averaged, each ring gives an estimate showing the reflecting the displacement of the

59
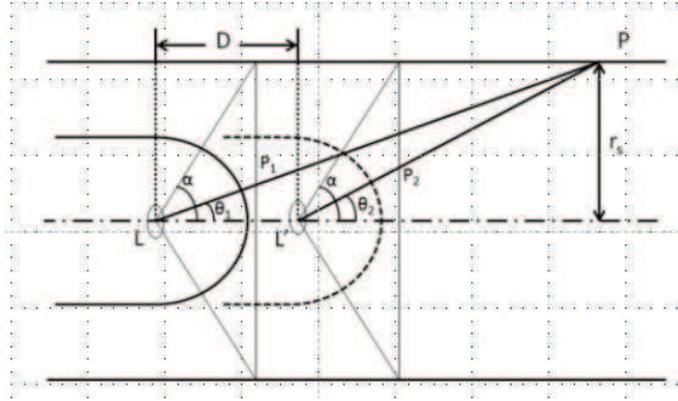
Figure 5.3: Estimating the displacement of FP in straight tube.

capsule. We use Figure 5.3 and Figure 5.4 to illustrate the procedure of estimating displacement of the capsule by measuring the estimate of each ring.

5.2.1 Displacement Estimation in Straight Tube

In Figure5.3, L refers to the initial position of the capsule and L' refers to the position after the capsule moves forward for a distance of D. During this process, the projection of a feature point P moves from P_1 to P_2, forming two angles $\theta 1$ and θ_2. According to our previous analysis, the displacement D can be calculated by the Equation 5.2.

$$D = \frac{r_s}{\tan \theta_1}(1 - \frac{\tan \theta_1}{\tan \theta_2})$$
(5.2)

5.2.2 Displacement Estimation in Contracted Tube

Figure 5.2b reflects the situation where the intestine is contracted and stick to the front cover of the capsule. In this scenario, as the capsule moves, the distance between the feature point and the lens of the capsule stays the same, yet still forming two angles θ_1 and θ_2. Plug in the expressions of θ_1 and θ_2, the displacement D can

be calculated by Equation 5.3.

$$D = r_s(\theta_2 - \theta_1) \tag{5.3}$$

where

One of the biggest influences of intestinal contraction on speed estimation algorithm is that objects in different regions of endoscopic images moves in different modes, compared to that without contraction. In next section, we give the test estimation results of both situations.

5.2.3 Speed Estimation

Finally the velocity of the capsule can be deduced as follows:

$$v = \frac{D}{\Delta t} \tag{5.4}$$

where D is deduced from Equation 5.2 and Equation 5.3; Δt is the time interval between two the capsule taking two adjacent frames.
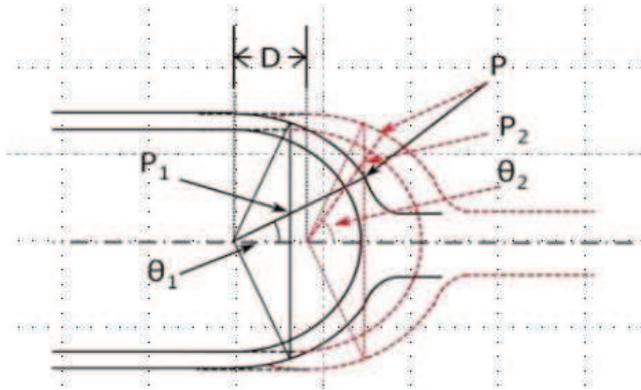
Figure 5.4: Estimating the displacement of FP in contracted tube. The walls of the tube is stick to the front cover, which means that the distance between a FP and the camera lens approximates the radius of the front cover.

5.3   Performance Evaluation

So far, two algorithms for speed estimation respectively in straight and contracted tube have been introduced . To clarify them, in this thesis, the algorithm for speed estimation in straight tube is defined as algorithm A while the algorithm for speed estimation in contracted tube is defined as algorithm B.

This section talks about four-folded experiments of using these algorithms in the virtual testbed introduced in chapter 3, which are: (1) using algorithm A in straight tube; (2) using algorithm A in contracted tube; (3) using algorithm B in straight tube; (4) using algorithm B in contracted tube. Experiment results closely match expectation.

5.3.1   Speed Estimation in a Straight Tube

A straight small intestine model has been created using the methodology in chapter 3. The straight tube is $100cm$ long, with a constant radius of $2cm$. The speed of the virtual camera is set to be $0.7mm/s$. During the transition of the camera, it takes pictures at resolution of $512 \times 512 pixels$. Field of view is 62°, which is the same as that of the wired camera used in the physical testbed, so α_i is 31°. To generate the nodes, the parameters are set as follows: $P = 7$, $Q = 128$, $r = 130$, $w = 1.1$.

The first step, feature point detection, is conducted using ASIFT method as discussed in section 5.1. Figure 5.5 shows the results. As expected, all the nodes moved outward to the border of the image, resulting in a larger radius of each ring. Also the structure of the rings is slightly distorted because of some error in detection.

Next step is to apply the speed estimation algorithm on the results of FP detection. First, the algorithm A is applied and the estimation result is shown in Figure 5.7a, which is attached to end of this chapter. Then, in order to illustrate the error brought by selecting the incorrect algorithm, the algorithm B is also applied on the straight tube and the estimation result is shown in Figure 5.7b.

As shown in Figure 5.7a, most of the estimates from all the feature point lie nearly on the real value which is normalized to 1. The variance of the estimates in small angle of view are larger than the variance in big angle of view, which is probably brought from the error of FP detection because when the angle of view is small, all contents are aggregated in small region of the endoscopic images and it is difficult to distinguish different FPs. Finally the average of the estimates is 0.9 which is pretty accurate.

As shown in Figure 5.7b, the estimates are far from the real value when the angle of view is small. This is because that when the small intestine is straight, as the camera moves for a little distance interval, the feature point that lies farther away from the camera moves much slower in the endoscopic images because of the projection principles [80] [81]. Thus it is safe to say that given two FPs extracted from the same images (which means their displacement in 3D space should be the same), the inner FP that are closer to the center of the image moves much slower that the outer FP. What if the small intestine is contracted? As shown in Figure 5.4, as the camera moves forward, the displacements of all the FPs on the images should

(a) Previous state   (b) Next state
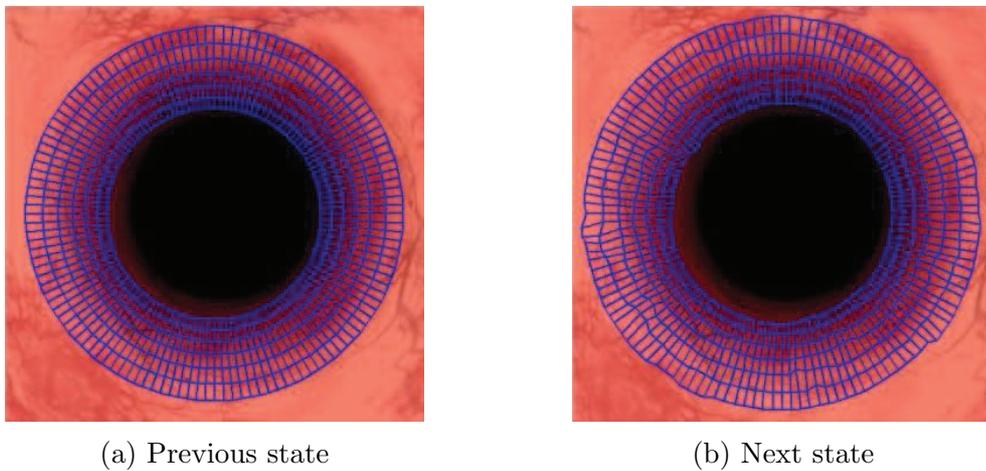
Figure 5.5: Feature point detection in a straight small intestine. Each node in the rings is regarded as a feature point, some of which doesn't have enough "feature" information for detect though. For each of these nodes, a threshold is set. If the detection result is far away from the original position, a real feature point near the node would substitute it for detection.

be the same because all FPs are moving along the hemispherical front cover of the capsule and thus it is easy to deduce from Equation 5.3 that the tilt angle of the FPs increase at a constant rate. Therefore, if the algorithm B which is only applicative to contracted tube is applied on straight tube, because the inner feature points moves slower, the algorithm will give the incorrect estimation that the camera is moving slowly.

5.3.2 Speed Estimation in a Contracted Tube

This subsection demonstrates the experiment results from contracted tube.

First and foremost a contracted small intestine is built using the proposed method. The diameter of the capsule is assumed as $12mm$. The radius of the contracted small intestine is $4mm$. For FP detection, the $r = 50$, $w = 1.26$ and other parameters are the same as those in previous subsection.

The results of FP detection are shown in Figure 5.6. As seen in the images, because of contraction, the walls of tube are closer to the lens of camera, resulting in a smaller black hole in the center, compared to the tube without contraction. Nodes of the rings moved a little longer if we compare Figure 5.6b and Figure 5.5b, which is corresponding to our previous analysis.

After applying the algorithm B which is designed for contracted small intestine, the results are shown in Figure 5.7c. As seen in the figure, most of the estimates lie around the real value of 1. On the left of the figure, when the angle of view is very small, the estimates are very small as well because at that angle, the walls of the small intestine is no longer stick to the front cover of the capsule and it becomes straight. So that estimates are similar to the left in Figure 5.7b.

Similarly, the algorithm A which is designed for is also applied to the contracted small intestine to test the error that can be brought by selecting the inappropriate algorithm. The results are shown in Figure 5.7d.

As shown in the figure, the estimates are tremendously far from the real value.

Because algorithm A assumes the small intestine is straight, it means that the FPs that are near the center of the image should have moved for a very short displacement. But the reality is that the walls of small intestine is hemispherical, which means that the FPs that are near the center of the image actually moves for a similar displacement than others. The displacements of those FPs are much larger than expectation of the algorithm. Thus the estimates become extremely large when the angle of view is small. On the other hand, the estimates are close the real values on the right end of the figure when the angle of view is relatively large.

5.4   Summary and Discussion

This chapter mainly discusses speed estimation of VCE inside small intestine. Based on ASIFT and MDR for FP detection, two algorithms respectively for estimating the speed of VCE inside straight and contracted small intestine have been introduced in details. Using the methodology in chapter 3, in the chapter, a model of straight small intestine and contracted small intestine are built for experiments. Two algorithms are applied to each of the model, which creates four scenarios. Based on the experiment results, it is safe to conclude that the proposed testbed is eligible for

(a) Previous state   (b) Next state
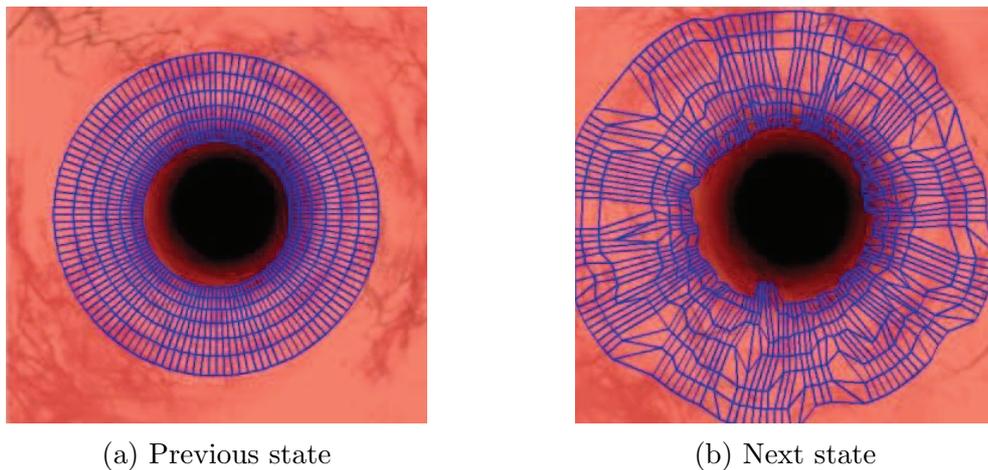
Figure 5.6: Feature point detection in the contracted small intestine. The detection strategy is the same as discussed in subsection 5.3.1, as shown in Figure 5.5.

experimentation of testing speed estimation algorithms.

This chapter also analyzes the errors that can be generated by selecting inappropriate algorithms for speed estimation. The conclusion is that if it is unknown whether the small intestine is contracted or not, using the outer FPs are safer than using the inner FPs, or in the other word, when averaging the estimates from all the FPs, the outer FPs should have more weights than that of inner FPs.

Chapter 4 introduces an method to measure the amount of intestinal contraction based on the size of the black hole. Therefore, combining the results of chapter 4 and of chapter 5, it is believable that a motion tracking algorithm that is adaptive to intestinal contraction could be developed based on our geometric models [82].
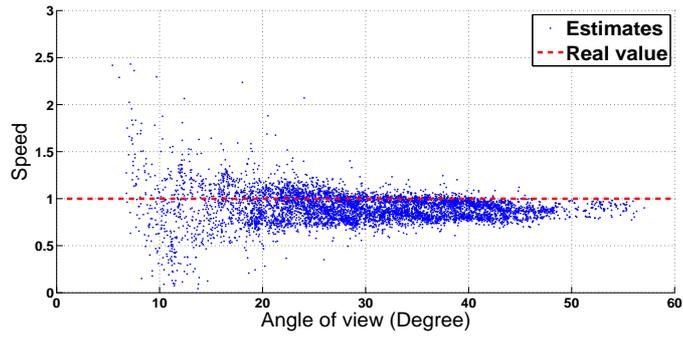
(a) Apply algorithm A in a straight tube.
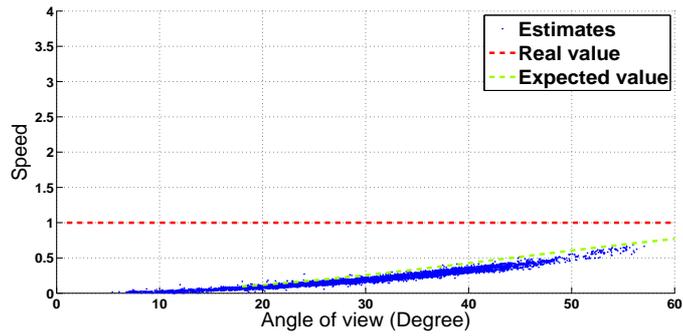
(b) Apply algorithm B in a straight tube.
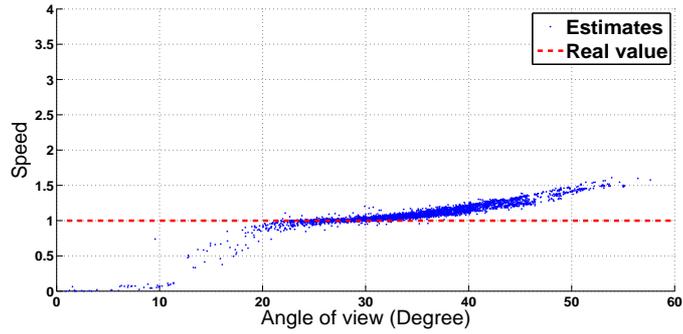
(c) Apply algorithm B in a contracted tube.
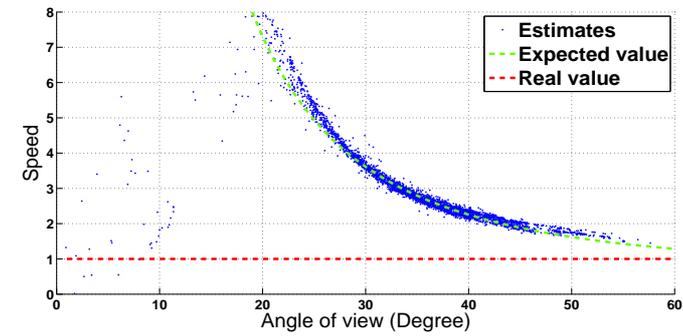
(d) Apply algorithm A in a contracted tube.

Figure 5.7: Speed estimation results.

Chapter 6

Conclusion and Future Work

This chapter presents the conclusion of the thesis and suggestions for future work.

6.1   Conclusion

In this thesis, we talk about using a testbed for design and performance evaluation of the motion tracking algorithm for localization of the VCE. A physical testbed and a virtual testbed have been presented perspectively in details. Based on the testbed, the intestinal contraction has been emulated and a geometric model for measuring the amount of contraction has been proposed. The algorithms for estimating the speed of the VCE have been implemented and examined in the testbed. By adding the contraction into the testbed, the influence of the intestinal contraction on the speed estimation algorithms have also been analyzed and a conclusion based on the experiment results has been presented.

By correlating each emulated endoscopic image to a specific location of the VCE, the testbed can provide accurate datasets in order to assist other algorithm designers who are working on visual localization technique to evaluate the performance of the algorithms. Based on the speed estimation results presented in this thesis, other researchers can improve their motion tracking algorithms by taking into account the influence of the intestinal contraction and making the algorithms adaptive to

different scenarios.

6.2   Future Work

One of the suggestions for future work is to add other features to the virtual testbed such as tumors or polyps. In [83], the author talks about using the specular component of illumination to detect polyps in the colon. Thus based on the virtual testbed, by adding a spherical object inside the small intestine and configuring its lighting properties of its material, the virtual testbed can be used to test the algorithms for detecting polyps. Also there are opportunities for improving the detection algorithm by combing the location information provided by the testbed.

Another suggestion for future work is to create a systematic testbed by immersing a 3D physical model into homogeneous tissues such as water, oil or other materials particularly designed for emulating the in-body environment. In this way, the testbed can be also used to test RF or MT localization techniques along with visual based techniques.

The virtual testbed can also be combined with the RF simulation environment to create a cyber localization testbed for performance evaluation of a hybrid (RF/visual) localization algorithm.

Appendix A

A Visual Based Motion Tracking Algorithm

The materials presented in this chapter draw substantially from results presented previously in:

1. Bao, Guanqun, Liang Mi, and Kaveh Pahlavan. "Emulation on motion tracking of endoscopic capsule inside small intestine." In 14th International Conference on Bioinformatics and Computational Biology, Las Vegas. 2013.

A.1 Motion Classification in Adjacent Video Frames

As shown in Figure A.1, if the inner walls of the small intestine is modeled as a cylindrical tube with a known diameter, the FP projected on the screen will change its location (from P_1 to P_2 and from Q_1 to Q_1) according to certain geometrical rules as the capsule moves. In Figure A.1a, the small intestine is straight while in Figure A.1b, the small intestine is bend. Once a feature point is detected on two adjacent video frames, a motion vector started from the previous location on the image to the next location. The motion vector is then inversely projected to 3D space to calculate the motion vector of the point in real 3D environment [84].

(a) Detect linear transition and rotation   (b) Detect tilting
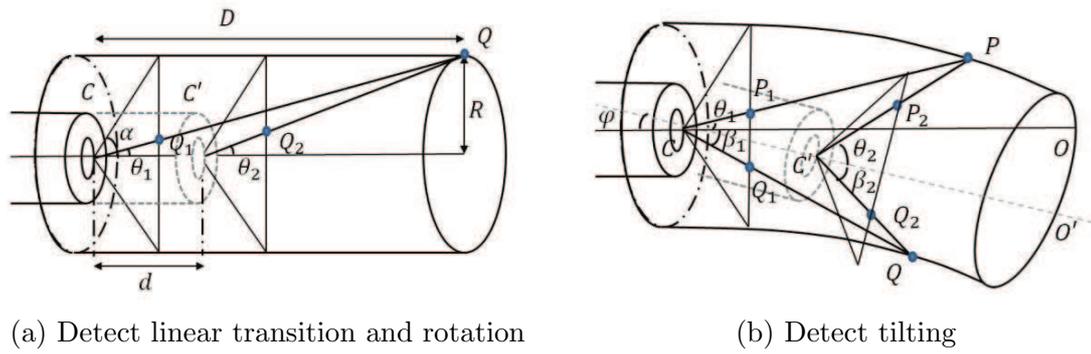
Figure A.1: Detection of the motion of the capsule based on the movement of the FP on the walls of small intestine.

Combining the results of all the FPs gives a overall estimation of the motion of the video capsule that causes the change in the video frames. In particular, the motion of the capsule is classified into four types: forward and backward transitions, rotate, and tilting. The corresponding scenarios are shown in Figure A.2. Finally, given a
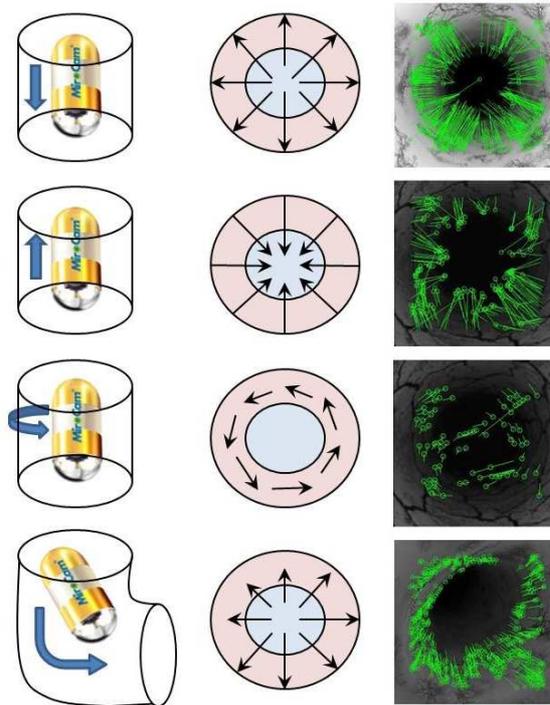
Figure A.2: Four different scenarios classified for visual based motion tracking, which are forward and backward transitions, rotation, and tilting.

start location of the video capsule, the location at any point of time can be calculated by adding motion vectors to the previous location, which makes the process simialr with Markov Chain [85] [86] [87].

A.2 Experiment Results using the Proposed Virtual Testbed

The motion tracking algorithm are then applied on the emulated images from the virtual testbed discussed in chapter 3. Particularly, the testbed shown in Figure 3.9 are used to emulate the image source. Figure A.3 shows the experiment results. The green line is the ground truth of the motion track of the virtual video capsule, which is a piece of the virtual testbed, and the yellow line is the reconstructed track. As shown in the figure, the error becomes increasingly larger as the capsule moves forward because the calculated location at each state totally depends on the location at the previous state, (which is one of the biggest limitation of this technique). To conquer this problem, a hybrid solution combining image localization technique and RF localization technique has been developed in our previous work [43].
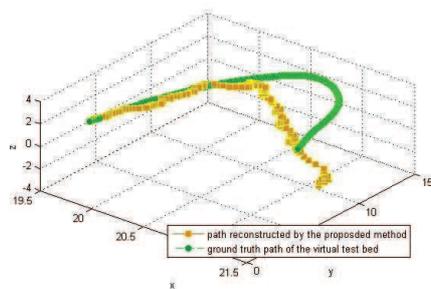
(a) Green line is the ground truth which is the shape of the virtual model; yellow line reflects the reconstruct of path of the virtual camera by the use of the motion tracking algorithm
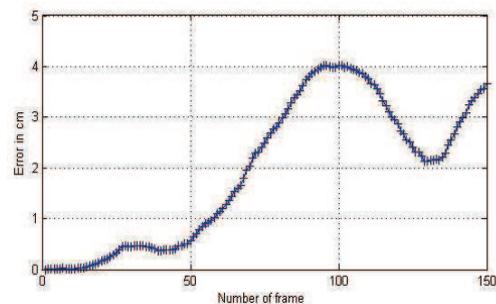
(b) Generally the error becomes larger as the virtual camera moves forward because the error brought in each step will accumulate. The amount and direction of the error are both unpredictable.

Figure A.3: Previous results from motion tracking of a virtual camera along a 3D virtual model.

Appendix B

Matlab Code Used for Speed Estimation

B.0.1 Main Function

```
/* main function */
clear
close all
I01=imread('frame1.jpg'); /* load first frame */
I02=imread('frame2.jpg'); /* load second frame */
/* load FP detection results */
C=importdata('ASIFTResult.txt');
[x,y,x0,y0,P,Q,r,w,I1,I2] = nodeMatching(I01,I02,C);
[J,d3] =tensionModeling(x,y,x0,y0,P,Q,r,w);
[Dpaverage1,Dqaverage1,Dp1,Dq1]=displacementEstimation1(x,y,x0,y0,P,Q);
[Dpaverage2,Dp2,Dqaverage2,Dq2]=displacementEstimation2(x,y,x0,y0,P,Q);
[r0,averager0]  = averagering(x0,y0,P,Q);
```

B.0.2   Function: nodeMatching

```
function [x,y,x0,y0,P,Q,r,w,I01,I02]  = nodeMatching(I01,I02,C)


/*------ASIFT FP aided match--------*/
clear
I01=imread('frame11.jpg'); %
I02=imread('frame22.jpg'); %
I1=255*im2double(I01);
I2=255*im2double(I02);
/*results are gained previously from ASIFT*/
C=importdata('match_ASIFT_frame11frame22.txt');


/*-------------set MDR parameters----------------*/
/*pq->xy*/
p=1;q=4;r=150
P=9;Q=128;
r=130;w=1.07;
[m,n,o] =size(I01);
/*-----------transform coordinates system---------*/
for q=1:Q
  for p=1:P
    x(p,q)=r*w^(p-1)*cos(2*pi*q/Q);
    y(p,q)=r*w^(p-1)*sin(2*pi*q/Q);
  end
end
x=x+13*ones(p,q);
y=y-15*ones(p,q);
/* -put the centre of the rings in the centre of the picture- */
```

```
x=floor(x)+m/2;
y=floor(y)+n/2;
[x0,y0]  = assignMDRnodestoFPs(C,x,y,P,Q);
```

B.0.3   Function: assignMDRnodestoFPs

```
function [coordinatesinsecondframex,coordinatesinsecondframey]...,
= assignMDRnodestoFPs(fpcoordinates,nodescoordinatesinfirstframex,nodescoordinate
fpcoordinates=floor(fpcoordinates+0.5*ones(size(fpcoordinates)));
C1=fpcoordinates(:,1);
C2=fpcoordinates(:,2);
C3=fpcoordinates(:,3);
C4=fpcoordinates(:,4);
x=nodescoordinatesinfirstframex;
y=nodescoordinatesinfirstframey;
for p=1:P
  for q=1:Q
    d2=sqrt((C1-x(p,q)*ones(length(C1),1)).^2+(C2-y(p,q)...,
    *ones(length(C1),1)).^2);
    //calculate the distance between a node and all other FPs
    l(p,q)=find(d2==min(d2),1);//find the closest FP for each node
    ll(p,q)=d2(l(p,q));
     /*use the coordinates of FPs in the second frame to
      estimate the coordinates of nodes in the second frame*/
    C01(p,q)=C3(l(p,q))+(x(p,q)-C1(l(p,q)));
    C02(p,q)=C4(l(p,q))+(y(p,q)-C2(l(p,q)));

  end
end
```

```
coordinatesinsecondframex=C01;

coordinatesinsecondframey=C02;
```

B.0.4   Function: assignMDRnodestoFPs2

```
function [d,dd,d0,d1,d2,theta1a,theta2a]
= assignMDRnodestoFPs2(coordinates,centerx,centery)
x0=centerx;
y0=centery;
C1=coordinates(:,1);
C2=coordinates(:,2);
C3=coordinates(:,3);
C4=coordinates(:,4);
l=length(C1);
for i=1:l
  d1(i)=sqrt((C1(i)-x0)^2+(C2(i)-y0)^2);
  //distance from FP to center, frame 1
  d2(i)=sqrt((C3(i)-x0)^2+(C4(i)-y0)^2);
  //distance from FP to center, frame 2
  tand1(i)=d1(i)/368;
  tand2(i)=d2(i)/368;
  theta1(i)=d1(i)/368*0.7854; pi/4=0.785398
  theta2(i)=d2(i)/368*0.7854;
  d(i)=10/tand1(i)*(1-tand1(i)/tand2(i));
  d(i)=16*cot(theta2(i)-theta1(i));
  d0(i)=10*(theta1(i)-theta2(i));
end
dd=mean(mean(d));
theta2a=theta2*180/pi;
```

```
theta1a=theta1*180/pi;
R=16;
r=16;
for i=1:1:89
  j1(i)=i/180*pi;
  j2(i)=(i+3.58)/180*pi;
  D1(i)=R/(tan(j1(i))*(1-tan(j1(i))/tan(j2(i))));
  D1(i)=R*(cot(j1(i))-cot(j2(i)));
  D2(i)=r*(j2(i)-j1(i));
end
```

B.0.5   Function: averagering

```
function [r0,averager0]  = averagering(x0,y0,P,Q)
r0=sqrt((x0-256*ones(P,Q)).^2+(y0-256*ones(P,Q)).^2);
averager0=mean(r0');
tantheta=averager0.*4.7./256;
theta=atan(tantheta);
end
```

B.0.6   Code for Generating a 3D Mesh of the Small Intestine

```
/*--------straight pipe with no rotation----*/
clear
x=1:100;
y=zeros(1,100);
z=zeros(1,100);
[X,Y,Z] =cylinder2(x,y,z,16*ones(1,100),200);
I0=imread('mask2.jpg');
csvwrite('surfacex.dat',X);
```

77

```
csvwrite('surfacey.dat',Y);
csvwrite('surfacez.dat',Z);
figure,surface(X,Y,Z,I0,'FaceColor','texturemap','EdgeColor',...,
'none','CDataMapping','direct');
hold on
axis equal
camproj('perspective');
camva(62);
camtarget([x(10),y(10),z(10)] );
campos([x(1),y(1),z(1)] );
set(figure(1),'position',[300   100   736   736] );
hold off
figure,surface(X,Y,Z,I1,'FaceColor','texturemap','EdgeColor'...,
,'none','CDataMapping','direct');
hold on
axis equal
camproj('perspective');
camva(62);
camtarget([x(100),y(100),z(100)] );
campos([x(2),y(2),z(2)] );
set(figure(2),'position',[600   100   736   736] );

/*-------contracted pipe with no rotation-------*/
clear
I4=imread('mask4.jpg');
x=1:101;
y=zeros(1,101);
z=zeros(1,101);
r1=16*ones(1,101);
```

```
r1(1)=16;
for i=2:14
  r1(i)=sqrt(16^2-(x(i))^2);
end
r1(15)=6.2;
r1(16:101)=5.5678*ones(1,86);
[X1,Y1,Z1] =cylinder2(x,y,z,r1,200);


r2=16*ones(1,101);
r2(1)=16;
r2(2)=16;
for i=3:15
  r2(i)=sqrt(16^2-(x(i)-1)^2);
end
r2(16)=6.2;
r2(17:101)=5.5678*ones(1,85);
[X2,Y2,Z2] =cylinder2(x,y,z,r2,200);
for i=1:201
  X2=spline(1:16,X(i,1:16),1:0.1:16);
  Y2=spline(1:16,Y(i,1:16),1:0.1:16);
  Z2=spline(1:16,Z(i,1:16),1:0.1:16);
  X1(i,:)=[X2,X(i,17:30)] ;
  Y1(i,:)=[Y2,Y(i,17:30)] ;
  Z1(i,:)=[Z2,Z(i,17:30)] ;
end
I0(:,1:328,:)=zeros(2048,328,3);
I1(:,1:348,:)=zeros(2048,348,3);
s=0;image center shift
p1=1;
```

```
p2=2;
u1=floor(0.03*ones(201,101-16)+rand(201,101-16));
u2=u1(:,2:101-16);
X2=X1(:,17:101).*u1;
Y2=Y1(:,17:101).*u1;
Z2=Z1(:,17:101).*u1;
X3=X1(:,18:101).*u2;
Y3=Y1(:,18:101).*u2;
Z3=Z1(:,18:101).*u2;
```

B.0.7   Function: cylinder2

```
function [X,Y,Z]=cylinder2(x,y,z,r,N,o)
X=[]; Y=[]; Z=[];
if nargin<5
  N=100;
end
x=x(:); y=y(:); z=z(:); r=r(:);
nx=length(x);ny=length(y);nz=length(z);nr=length(r);
an=[nx ny nz nr];
if ~ismember(diff(an),[0 0 0],'rows')
  disp(' ')
  disp('x, y, z, r must have the same length!')
else
  if nx<2
    disp(' ')
    disp('The length of x must be greater than 1!')
  else
    if nargin<6
```

```
  o=ones(nx,2);
else
  [o1,o2]=size(o);
  if o2>o1
    o=o';
  end
end
C=[x y z];D=diff(C);E=zeros(nx-1,3);
for i=1:nx-1
  if norm(D(i,:))>0
    E(i,:)=D(i,:)/norm(D(i,:));
  else
    E(i,:)=[0 0 0];
  end
end
if norm(C(1,:)-C(nx,:))<1e-10 && norm(cross(E(1,:),E(nx-1,:)))>0
  Closed=1;nxx=nx+1;E=[E;E(1,:)];
else
  Closed=0;nxx=nx;
end
f=linspace(0,2*pi,N+1);
xcc=cos(f);ycc=sin(f);zcc=zeros(size(f));
for i=1:nx
  if i==1
    if ~Closed
      d=[];k=i;
      while k<nx-1
        if norm(cross(E(k,:),E(k+1,:)))==0
          k=k+1;d=[d k];
```

```
    else
      break
    end
  end
  if norm(E(1,:))==0;
    vz=E(2,:);
  else
    vz=E(1,:);
  end
  if k==nx-1
    if norm(cross([0 0 1],vz))~=0
      va=cross([0 0 1],vz);
    else
      va=cross([1 1 1],vz);
    end
  else
    va=cross(E(k+1,:),vz);
  end
  vy=va/norm(va);vx=cross(vy,vz);V=[vx;vy;vz];
  Vp=V;Vpp=V;alf=0;
else
  d=[];
  vb=(E(1,:)+E(nx-1,:))/2;vz=vb/norm(vb);
  va=cross(E(1,:),E(nx-1,:));vy=va/norm(va);
  vx=cross(vy,vz);V=[vx;vy;vz];Vpp=V;
  alf=acos(E(1,:)*E(nx-1,:)');
  if abs(alf>3*pi/4)
    alf=0;
  end
```

```
      end
else
   if ismember(i,d)
      V=Vp;alf=0;
   else
      d=[];
      k=i;
      while k<nx-1
         if norm(cross(E(k,:),E(k+1,:)))==0
            k=k+1;
            d=[d k];
         else
            break
         end
      end
      if ~isempty(d) || i==nx
         if norm(E(i-1,:))==0;
            vz=E(i-2,:);
         else
            if i==nx
               vz=E(i-1,:);
            else
               vz=E(i,:);
            end
         end
         va=Vpp(2,:);vy=va/norm(va);vx=cross(vy,vz);
         V=[vx;vy;vz];Vp=V;alf=0;
      end
      if i<nxx
```

```
        vb=(E(i,:)+E(i-1,:))/2;vz=vb/norm(vb);
        va=cross(E(i,:),E(i-1,:)); vy=va/norm(va);
        vx=cross(vy,vz); V=[vx;vy;vz];
        ang=acos(vy*Vpp(2,:)');Vang=cross(vy,Vpp(2,:));
        if Vang*vz'>0
          ang=-ang;
        end
        A=[cos(ang) sin(ang); -sin(ang) cos(ang)];
        xy=A*[xcc;ycc];xcc=xy(1,:);ycc=xy(2,:);
        Vpp=V;alf=acos(E(i,:)*E(i-1,:)');
        if abs(alf>3*pi/4)
          alf=0;
        end
      end
    end
  end
  xc=o(i,1)*r(i)/cos(alf/2)*xcc;yc=o(i,2)*r(i)*ycc;
  xyz=[xc;yc;zcc];M=pinv(V);
  xyz1=M*xyz+repmat([x(i);y(i);z(i)],1,N+1);
  X(:,i)=xyz1(1,:)';Y(:,i)=xyz1(2,:)';Z(:,i)=xyz1(3,:)';
  X=real(X);Y=real(Y);Z=real(Z);
    end
  end
end
```

Appendix C

Full Publication List

C.1 Related to this Thesis

1. Mi, Liang, Guanqun Bao, and Kaveh Pahlavan. "Design and validation of a virtual environment for experimentation inside the small intestine", In Proceedings of the 8th International Conference on Body Area Networks, pp. 35-40. ICST (Institute for Computer Sciences, Social-Informatics and Telecommunications Engineering), 2013.

2. Mi, Liang, Guanqun Bao, and Kaveh Pahlavan. "Geometric Estimation of Intestinal Contraction for Motion Tracking of Video Capsule Endoscope", In Proceedings of SPIE Volume 9036, Medical Imaging 2014: Image-Guided Procedures, Robotic Interventions, and Modeling, San Diego, 2014.

3. Bao, Guanqun, Liang Mi, and Kaveh Pahlavan. "Emulation on motion tracking of endoscopic capsule inside small intestine." In 14th International Conference on Bioinformatics and Computational Biology, Las Vegas. 2013.

4. Bao, Guanqun, Liang Mi, and Kaveh Pahlavan. "A video aided RF localization technique for the wireless capsule endoscope (WCE) inside small intestine." In Proceedings of the 8th International Conference on Body Area Net-

works, pp. 55-61. ICST (Institute for Computer Sciences, Social-Informatics and Telecommunications Engineering), 2013.

5. K. Pahlavan, G. Bao and L. Mi, "Body-SLAM: Simultaneous Localization and Mapping inside the Human Body", keynote speech, IEEE/ACM 8th International Conference on Body Area Networks (BodyNets), Boston, MA, September 30-October 2, 2013.

C.2   Not Related to this Thesis

1. Zhou, Shuang, Liang Mi, etc. "Building detection in Digital surface model." In Proceedings of Imaging Systems and Techniques (IST), 2013 IEEE International Conference on, pp. 194 - 199, 2013.

2. Yunzhou Zhang, Huiyu Liu, Wenyan Fu, Aichun Zhou and Liang Mi. "Localization algorithm for GSM mobiles based on RSSI and Pearson's correlation coefficient." In Proceedings of Consumer Electronics (ICCE), 2014 IEEE International Conference on, pp. 284 - 285, 2014.

References

[1] Y. Ye, *Bounds on RF cooperative localization for video capsule endoscopy.* Diploma dissertation, Worcester Polytechnic Institute, Worcester, Massachussets, USA, 6 2013.

[2] R. Fu, "Empirical rf propagation modeling of human body motions for activity classification," diploma thesis, Worcester Polytechnic Institute, Worcester, Massachussets, USA, 1 2013.

[3] W. A. Voderholzer, J. Beinhoelzl, P. Rogalla, S. Murrer, G. Schachschal, H. Lochs, and M. A. Ortner, "Small bowel involvement in crohns disease: a prospective comparison of wireless capsule endoscopy and computed tomography enteroclysis," *Gut*, vol. 54.3, pp. 369–373, 2005.

[4] M. K. OConnor and B. J. Kemp, "Single-photon emission computed tomography/computed tomography: basic instrumentation and innovations," *Seminars in nuclear medicine*, vol. 36, no. 4, pp. 258–266, 2006.

[5] S. W. Heijmink, J. J. Futterer, T. Hambrock, S. Takahashi, T. W. Scheenen, H. J. Huisman, and C. A. H. de Kaa et al, "Prostate cancer: Body-array versus endorectal coil mr imaging at 3 tcomparison of image quality, localization, and staging performance 1," *Radiology*, vol. 244.1, pp. 184–195, 2007.

[6] G. Iddan, G. Meron, A. Glukhovsky, and P. Swain, "Wireless capsule endoscopy," *"Nature*, vol. 405, p. 417, 2000.

[7] P. Swain, "Wireless capsule endoscopy," *Gut*, vol. 52, no. suppl 4, pp. iv48–iv50, 2003.

[8] D. O. Faigel and D. R. Cave, *Capsule Endoscopy.* Saunders Elsevier, 2005.

[9] C. Ell, S. Remke, A. May, L. Helou, R. Henrich, and G. Mayer, "The first prospective controlled trial comparing wireless capsule endoscopy with push enteroscopy in chronic gastrointestinal bleeding," *Endoscopy*, vol. 34.9, pp. 685–689, 2002.

[10] P. Swain, G. J. Iddan, G. Meron, and A. Glukhovsky, "Wireless capsule endoscopy of the small bowel: development, testing, and first human trials," in

EOS/SPIE European Biomedical Optics Week, pp. 19-23. International Society for Optics and Photonics, (Amsterdam, Netherlands), 7 2000.

[11] M. Appleyard, Z. Fireman, A. Glukhovsky, H. Jacob, R. Shreiver, S. Kadirka-manathan, A. Lavy, S. Lewkowicz, E. Scapa, R. Shofti, *et al.*, "A randomized trial comparing wireless capsule endoscopy with push enteroscopy for the detection of small-bowel lesions," *Gastroenterology*, vol. 119, no. 6, pp. 1431–1438, 2000.

[12] B. S. Lewis and P. Swain, "Capsule endoscopy in the evaluation of patients with suspected small intestinal bleeding: results of a pilot study," *Gastrointestinal endoscopy*, vol. 56.3, pp. 349–353, 2000.

[13] G. Bresci, G. Parisi, M. Bertoni, E. Tumino, and A. Capria, "The role of video capsule endoscopy for evaluating obscure gastrointestinal bleeding: usefulness of early use," *Journal of gastroenterology*, vol. 40.3, pp. 256–259, 2005.

[14] S. Liangpunsakul, V. Chadalawada, D. K. Rex, D. Maglinte, and J. Lappas, "Wireless capsule endoscopy detects small bowel ulcers in patients with normal results from state of the art enteroclysis," *The American journal of gastroenterology*, vol. 98.6, pp. 1295–1298, 2003.

[15] A. Culliford, J. Daly, B. Diamond, M. Rubin, and P. H. Green, "The value of wireless capsule endoscopy in patients with complicated celiac disease," *Gastrointestinal endoscopy*, vol. 62.1, pp. 55–61, 2005.

[16] E. Dubcenco, K. N. Jeejeebhoy, R. Petroniene, S. jiang Tang, A. H. Zalev, G. W. Gardiner, , and J. P. Baker, "Capsule endoscopy findings in patients with established and suspected small-bowel crohn's disease: correlation with radiologic, endoscopic, and histologic findings," *Gastrointestinal endoscopy*, vol. 62.4, pp. 538–544, 2005.

[17] S. Tanaka, K. Mitsui, K. Shirakawa, A. Tatsuguchi, T. Nakamura, Y. Hayashi, M. Jakazoe, C. Sakamoto, and A. Terano, "Successful retrieval of video capsule endoscopy retained at ileal stenosis of crohns disease using doubleballoon endoscopy," *Journal of gastroenterology and hepatology*, vol. 21.5, pp. 922–923, 2006.

[18] G. Costamagna, S. K. Shah, M. E. Riccioni, F. Foschia, M. Mutignani, V. Perri, A. Vecchioli, M. G. Brizi, A. Picciocchi, and P. Marano, "A prospective trial comparing small bowel radiographs and video capsule endoscopy for suspected small bowel disease," *Gastroenterology*, vol. 123, no. 4, pp. 999–1005, 2002.

[19] S. K. Gölder, A. G. Schreyer, E. Endlicher, S. Feuerbach, J. Schölmerich, F. Kullmann, J. Seitz, G. Rogler, and H. Herfarth, "Comparison of capsule endoscopy and magnetic resonance (mr) enteroclysis in suspected small bowel

disease," *International journal of colorectal disease*, vol. 21, no. 2, pp. 97–104, 2006.

[20] H.-G. Lee, M.-K. Choi, and S.-C. Lee, "Motion analysis for duplicate frame removal in wireless capsule endoscope," in *SPIE Medical Imaging*, pp. 79621T–79621T, International Society for Optics and Photonics, 2011.

[21] Y. Liu, T. Tillo, J. Xiao, E. Lim, and Z. Wang, "2d to cylindrical inverse projection of the wireless capsule endoscopy images," in *Image and Signal Processing (CISP), 2011 4th International Congress on*, vol. 1, pp. 1–5, IEEE, 2011.

[22] G. Bao, L. Mi, and K. Pahlavan, "Emulation on motion tracking of endoscopic capsule inside small intestine," in *14th International Conference on Bioinformatics and Computational Biology*, (Las Vegas, Nevada, USA), 7 2013.

[23] G. Bao and K. Pahlavai, "Motion estimation of the endoscopy capsule using region-based kernel svm classifier," in *Electro/Information Technology (EIT), 2013 IEEE International Conference on*, pp. 1–5, IEEE, 2013.

[24] G. Bao, Y. Ye, U. Khan, X. Zheng, and K. Pahlavan, "Modeling of the movement of the endoscopy capsule inside gi tract based on the captured endoscopic images," in *Proceedings of the IEEE International Conference on Modeling, Simulation and Visualization Methods, MSV*, vol. 12, 2012.

[25] R. Fu, G. Bao, and K. Pahlavan, "Activity classification with empirical rf propagation modeling in body area networks," in *Proceedings of the 8th International Conference on Body Area Networks*, pp. 296–301, ICST (Institute for Computer Sciences, Social-Informatics and Telecommunications Engineering), 2013.

[26] J. He, Y. Geng, Y. Wan, S. Li, and K. Pahlavan, "A cyber physical test-bed for virtualization of rf access environment for body sensor network," 2013.

[27] J. He, Y. Geng, and K. Pahlavan, "Modeling indoor toa ranging error for body mounted sensors," in *Personal Indoor and Mobile Radio Communications (PIMRC), 2012 IEEE 23rd International Symposium on*, pp. 682–686, IEEE, 2012.

[28] K. Pahlavan, G. Bao, Y. Ye, S. Makarov, U. Khan, P. Swar, D. Cave, A. Karellas, P. Krishnamurthy, and K. Sayrafian, "Rf localization for wireless video capsule endoscopy," *International Journal of Wireless Information Networks*, vol. 19, no. 4, pp. 326–340, 2012.

[29] Y. Geng, *Modeling of Time-of-arrival for CM4 Body Area Networks Channel*. PhD thesis, Worcester Polytechnic Institute, 2013.

[30] Y. Geng, J. Chen, and K. Pahlavan, "Motion detection using rf signals for the first responder in emergency operations: A phaser project," in *Personal Indoor and Mobile Radio Communications (PIMRC), 2013 IEEE 24th International Symposium on*, pp. 358–364, IEEE, 2013.

[31] Y. Ye, P. Swar, K. Pahlavan, and K. Ghaboosi, "Accuracy of rss-based rf localization in multi-capsule endoscopy," *International Journal of Wireless Information Networks*, vol. 19, no. 3, pp. 229–238, 2012.

[32] Y. Geng, Y. Wan, J. He, and K. Pahlavan, "An empirical channel model for the effect of human body on ray tracing," in *Personal Indoor and Mobile Radio Communications (PIMRC), 2013 IEEE 24th International Symposium on*, pp. 47–52, IEEE, 2013.

[33] Z. Liu, J. Chen, U. Khan, B. Alkandari, and K. Pahlavan, "Wideband characterization of rf propagation for toa localization of wireless video capsule endoscope inside small intestine," in *Personal Indoor and Mobile Radio Communications (PIMRC), 2013 IEEE 24th International Symposium on*, pp. 326–331, IEEE, 2013.

[34] Y. Geng, H. Deng, *et al.*, "Modeling the effect of human body on toa ranging for indoor human tracking with wrist mounted sensor," in *Wireless Personal Multimedia Communications (WPMC), 2013 16th International Symposium on*, pp. 1–6, IEEE, 2013.

[35] Y. Geng, J. He, and K. Pahlavan, "Modeling the effect of human body on toa based indoor human tracking," *International Journal of Wireless Information Networks*, vol. 20, no. 4, pp. 306–317, 2013.

[36] Y. Ma, L. Zhou, K. Liu, and J. Wang, "Iterative phase reconstruction and weighted localization algorithm for indoor rfid-based localization in nlos environment," 2014.

[37] Y. Huang, J. Benesty, G. W. Elko, and R. M. Mersereati, "Real-time passive source localization: A practical linear-correction least-squares approach," *Speech and Audio Processing, IEEE Transactions on*, vol. 9.8, pp. 943–956, 2001.

[38] S. Li, Y. Geng, J. He, and K. Pahlavan, "Analysis of three-dimensional maximum likelihood algorithm for capsule endoscopy localization," in *Biomedical Engineering and Informatics (BMEI), 2012 5th International Conference on*, pp. 721–725, IEEE, 2012.

[39] C. Hu, M.-H. Meng, , and M. Mandal, "The calibration of 3-axis magnetic sensor array system for tracking wireless capsule endoscope," in *Intelligent Robots*

and Systems, 2006 IEEE/RSJ International Conference on, (beijing, China), 10 2006.

[40] P. New, B. Rosen, T. J. Brady, F. Buonanno, J. Kistler, C. Burt, W. Hinshaw, J. Newhouse, G. Pohost, and J. Taveras, "Potential hazards and artifacts of ferromagnetic and nonferromagnetic surgical and dental materials and devices in nuclear magnetic resonance imaging.," *Radiology*, vol. 147, no. 1, pp. 139–148, 1983.

[41] W. Weitschies, O. Kosch, H. Mnnikes, and L. Trahms, "Magnetic marker monitoring: an application of biomagnetic measurement instrumentation and principles for the determination of the gastrointestinal behavior of magnetically marked solid dosage forms," *Advanced drug delivery reviews*, vol. 57.8, pp. 1210–1222, 2005.

[42] C. Hu, M. Q.-H. Meng, and M. Mandal, "Efficient magnetic localization and orientation technique for capsule endoscopy," *International Journal of Information Acquisition*, vol. 2, no. 01, pp. 23–36, 2005.

[43] G. Bao, L. Mi, and K. Pahlavan, "A video aided rf localization technique for the wireless capsule endoscope (wce) inside small intestine," in *Proceedings of the 8th International Conference on Body Area Networks*, pp. 55–61, ICST (Institute for Computer Sciences, Social-Informatics and Telecommunications Engineering), 2013.

[44] J. Bulat, K. Duda, M. Duplaga, R. Fraczek, A. Skalski, M. Socha, P. Turcza, and T. Zielinski, "Data processing tasks in wireless gi endoscopy: image-based capsule localization & navigation and video compression," in *Engineering in Medicine and Biology Society, 2007. EMBS 2007. 29th Annual International Conference of the IEEE*, pp. 2815–2818, IEEE, 2007.

[45] C. S. Bell, K. L. Obstein, and P. Valdastri, "Image partitioning and illumination in image-based pose detection for teleoperated flexible endoscopes," *Artificial intelligence in medicine*, vol. 59, no. 3, pp. 185–196, 2013.

[46] D. G. Lowe, "Object recognition from local scale-invariant features," in *Computer vision, 1999. The proceedings of the seventh IEEE international conference on*, vol. 2, pp. 1150–1157, IEEE, 1999.

[47] J.-M. Morel and G. Yu, "Asift: A new framework for fully affine invariant image comparison," *SIAM Journal on Imaging Sciences*, vol. 2, no. 2, pp. 438–469, 2009.

[48] H. Bay, T. Tuytelaars, and L. Van Gool, "Surf: Speeded up robust features," in *Computer Vision–ECCV 2006*, pp. 404–417, Springer, 2006.

[49] K. Pahlavan, G. Bao, and L. Mi, "Body-slam: Simultaneous localization and mapping inside the human body," *keynote speech, IEEE/ACM 8th International Conference on Body Area Networks (BodyNets)*, 10 2013.

[50] L. France, J. Lenoir, A. Angelidis, P. Meseure, M.-P. Cani, F. Faure, and C. Chaillou, "A layered model of a virtual human intestine for surgery simulation," *Medical image analysis*, vol. 9, no. 2, pp. 123–132, 2005.

[51] L. Mi, G. Bao, and K. Pahlavan, "Design and validation of a virtual environment for experimentation inside the small intestine," in *Proceedings of the 8th International Conference on Body Area Networks*, pp. 35–40, ICST (Institute for Computer Sciences, Social-Informatics and Telecommunications Engineering), 2013.

[52] G. Chen, F. Thomann, M. T. Pham, M. Bétemps, and T. Redarce, "Modeling and control of a colonoscopic tip under disturbance of the insertion of colonoscope," in *Intelligent Robots and Systems, 2004.(IROS 2004). Proceedings. 2004 IEEE/RSJ International Conference on*, vol. 4, pp. 3315–3320, IEEE, 2004.

[53] L. B. Gerson and J. Van Dam, "Wireless capsule endoscopy and double-balloon enteroscopy for the diagnosis of obscure gastrointestinal bleeding," *Techniques in vascular and interventional radiology*, vol. 7, no. 3, pp. 130–135, 2004.

[54] P. Swain and A. Fritscher-Ravens, "Role of video endoscopy in managing small bowel disease," *Gut*, vol. 53, no. 12, pp. 1866–1875, 2004.

[55] I. Bricault, G. Ferretti, and P. Cinquin, "Registration of real and ct-derived virtual bronchoscopic images to assist transbronchial biopsy," *Medical Imaging, IEEE Transactions on*, vol. 17, no. 5, pp. 703–714, 1998.

[56] H. Çakmak and U. Kühnapfel, "Animation and simulation techniques for vr-training systems in endoscopic surgery," in *Computer Animation and Simulation 2000*, pp. 173–185, Springer, 2000.

[57] K. Mori, D. Deguchi, J.-i. Hasegawa, Y. Suenaga, J.-i. Toriwaki, H. Takabatake, and H. Natori, "A method for tracking the camera motion of real endoscope by epipolar geometry analysis and virtual endoscopy system," in *Medical Image Computing and Computer-Assisted Intervention–MICCAI 2001*, pp. 1–8, Springer, 2001.

[58] K. Mori, D. Deguchi, J. Sugiyama, Y. Suenaga, J.-i. Toriwaki, C. R. Maurer Jr, H. Takabatake, and H. Natori, "Tracking of a bronchoscope using epipolar geometry analysis and intensity-based image registration of real and virtual endoscopic images," *Medical Image Analysis*, vol. 6, no. 3, pp. 321–336, 2002.

[59] L. Raghupathi, L. Grisoni, F. Faure, D. Marchal, M.-P. Cani, and C. Chaillou, "An intestinal surgery simulator: Real-time collision processing and visualization," *Visualization and Computer Graphics, IEEE Transactions on*, vol. 10, no. 6, pp. 708–718, 2004.

[60] P. M. Szczypiński, R. D. Sriram, P. V. Sriram, and D. N. Reddy, "A model of deformable rings for interpretation of wireless capsule endoscopic videos," *Medical Image Analysis*, vol. 13, no. 2, pp. 312–324, 2009.

[61] H. Zhou, G. Alici, T. D. Than, and W. Li, "Modeling and experimental investigation of rotational resistance of a spiral-type robotic capsule inside a real intestine," *Mechatronics, IEEE/ASME Transactions on*, vol. 18, no. 5, pp. 1555–1562, 2013.

[62] J. L. Gorlewicz, S. Battaglia, B. F. Smith, G. Ciuti, J. Gerding, A. Menciassi, K. L. Obstein, P. Valdastri, and R. Webster, "Wireless insufflation of the gastrointestinal tract," *Biomedical Engineering, IEEE Transactions on*, vol. 60, no. 5, pp. 1225–1233, 2013.

[63] P. Valdastri, R. J. Webster, C. Quaglia, M. Quirini, A. Menciassi, and P. Dario, "A new mechanism for mesoscale legged locomotion in compliant tubular environments," *Robotics, IEEE Transactions on*, vol. 25, no. 5, pp. 1047–1057, 2009.

[64] S. Hosseini, M. Mehrtash, and M. B. Khamesee, "Design, fabrication and control of a magnetic capsule-robot for the human esophagus," *Microsystem technologies*, vol. 17, no. 5-7, pp. 1145–1152, 2011.

[65] P. Rogalla, J. T. van Scheltinga, A. Aschoff, and B. Hamm, *Virtual endoscopy and related 3D techniques*. Springer, 2000.

[66] P. J. Pickhardt, J. R. Choi, I. Hwang, J. A. Butler, M. L. Puckett, H. A. Hildebrandt, R. K. Wong, P. A. Nugent, P. A. Mysliwiec, and W. R. Schindler, "Computed tomographic virtual colonoscopy to screen for colorectal neoplasia in asymptomatic adults," *New England Journal of Medicine*, vol. 349, no. 23, pp. 2191–2200, 2003.

[67] L. M. Pusanik, M. J. D. Malley, R. B. Jeffrey Jr, D. I. Glazer, and S. Napel, "Automated polyp detector for ct colonography: Feasibility study1," *Radiology*, vol. 216, pp. 284–290, 2000.

[68] K. Inamoto, K. Kouzai, T. Ueeda, and T. Marukawa, "Ct virtual endoscopy of the stomach: comparison study with gastric fiberscopy," *Abdominal imaging*, vol. 30, no. 4, pp. 473–479, 2005.

[69] H. R. Roth, T. E. Hampshire, E. Helbren, M. Hu, R. Vega, S. Halligan, and D. J. Hawkes, "Computer-assisted polyp matching between optical colonoscopy and ct colonography: a phantom study," in *SPIE Medical Imaging*, pp. 903609–903609, International Society for Optics and Photonics, 2014.

[70] G. Imaging, "Pillcam sb 3 capsule endoscopy." `http://http://www.givenimaging.com/en-int/Innovative-Solutions/Capsule-Endoscopy/Pillcam-SB/PillCam-SB-3/Pages/default.aspx`.

[71] R. Carta, M. Sfakiotakis, N. Pateromichelakis, J. Thoné, D. Tsakiris, and R. Puers, "A multi-coil inductive powering system for an endoscopic capsule with vibratory actuation," *Sensors and Actuators A: Physical*, vol. 172, no. 1, pp. 253–258, 2011.

[72] D. J. Mirota, A. Uneri, S. Schafer, S. Nithiananthan, D. D. Reh, G. L. Gallia, R. H. Taylor, G. D. Hager, and J. H. Siewerdsen, "High-accuracy 3d image-based registration of endoscopic video to c-arm cone-beam ct for image-guided skull base surgery," in *SPIE Medical Imaging*, pp. 79640J–79640J, International Society for Optics and Photonics, 2011.

[73] K. Ogden, N. Ordway, D. Diallo, G. Tillapaugh-Fay, and C. Asian, "Dimensional accuracy of 3d printed vertebra," in *SPIE Medical Imaging*, pp. 903629–903629, International Society for Optics and Photonics, 2014.

[74] TurboSquid, "Anatomy intestine." `http://www.turbosquid.com/3d-models/3d-c4d-colon-small-intestine/571181`, 2010. Online; accessed Nov 27, 2010.

[75] M. K. Agoston, *Computer graphics and geometric modeling*, vol. 2. Springer, 2005.

[76] E. Angle and D. Shreiner, "Interactive computer graphics: A topdown approach with shader-based opengl," 2011.

[77] F. Hill and S. Kelley, *Computer Graphics Using OpenGL, 3/E*. Pearson, 2007.

[78] X. Wang, M.-H. Meng, and Y. Chan, "Physiological factors of the small intestine in design of active capsule endoscopy," in *Engineering in Medicine and Biology Society, 2005. IEEE-EMBS 2005. 27th Annual International Conference of the*, pp. 2942–2945, IEEE, 2006.

[79] L. Mi, G. Bao, and K. Pahlavan, "Geometric estimation of intestinal contraction for motion tracking of video capsule endoscope," in *2014 SPIE Medical Image: Image-Guided Procedures, Robotic Interventions, and Modeling*, vol. 9036, SPIE, 2014.

[80] C. Cruz-Neira, D. J. Sandin, and T. A. DeFanti, "Surround-screen projection-based virtual reality: the design and implementation of the cave," in *Proceedings of the 20th annual conference on Computer graphics and interactive techniques*, pp. 135–142, ACM, 1993.

[81] R. C. Nelson, "Qualitative detection of motion by a moving observer," *International journal of computer vision*, vol. 7, no. 1, pp. 33–46, 1991.

[82] G. Bao, "Body-slam: Simultaneous localization and mapping inside the human body," *PhD Dissertation*, 2014.

[83] J. Bernal, J. Sánchez, and F. Vilarino, "Impact of image preprocessing methods on polyp localization in colonoscopy frames," in *Engineering in Medicine and Biology Society (EMBC), 2013 35th Annual International Conference of the IEEE*, pp. 7350–7354, IEEE, 2013.

[84] S. Sathyanarayana, S. Thambipillai, and C. T. Clarke, "Real time tracking of camera motion through cylindrical passages," in *Digital Signal Processing, 2007 15th International Conference on*, pp. 455–458, IEEE, 2007.

[85] X. Zhou, Y. Lu, J. Lu, and J. Zhou, "Abrupt motion tracking via intensively adaptive markov-chain monte carlo sampling," *Image Processing, IEEE Transactions on*, vol. 21, no. 2, pp. 789–801, 2012.

[86] S. Oh, S. Russell, and S. Sastry, "Markov chain monte carlo data association for general multiple-target tracking problems," in *Decision and Control, 2004. CDC. 43rd IEEE Conference on*, vol. 1, pp. 735–742, IEEE, 2004.

[87] Q. Yu, G. Medioni, and I. Cohen, "Multiple target tracking using spatio-temporal markov chain monte carlo data association," in *Computer Vision and Pattern Recognition, 2007. CVPR'07. IEEE Conference on*, pp. 1–8, IEEE, 2007.